HHS Public Access

Author manuscript

Cell Rep. Author manuscript; available in PMC 2024 February 16.

Published in final edited form as:

Cell Rep. 2023 December 26; 42(12): 113461. doi:10.1016/j.celrep.2023.113461.

Identification of a Targetable JAK-STAT Enriched Androgen Receptor (AR) and AR Splice Variant Positive Triple Negative Breast Cancer Subtype

Sarah Asemota[1], **Wendy Effah**[1], **Kirsten L. Young**[1], **Jeremiah Holt**[1], **Linnea Cripe**[2], **Suriyan Ponnusamy**[1], **Thirumagal Thiyagarajan**[1], **Dong-Jin Hwang**[3], **Yali He**[3], **Keely Mcnamara**[4], **Daniel Johnson**[5], **Yinan Wang**[6], **Brandy Grimes**[7], **Yekta Khosrosereshki**[1], **TJ Hollingsworth**[8], **Martin D. Fleming**[2], **Frances E. Pritchard**[2], **Ashley Hendrix**[2], **Farhan Khan**[9], **Meiyun Fan**[6], **Liza Makowski**[1,10], **Zheng Yin**[11], **Hironobu Sasano**[4], **D. Neil Hayes**[1,10], **Lawrence M. Pfeffer**[6,10], **Duane D. Miller**[3,10], **Ramesh Narayanan**[1,10,*]

[1]Department of Medicine, College of Medicine, University of Tennessee Health Science Center, Memphis, TN 38103, USA.

[2]Department of Surgery, College of Medicine, University of Tennessee Health Science Center, Memphis, TN 38103, USA.

[3]Department of Pharmaceutical Sciences, College of Pharmacy, University of Tennessee Health Science Center, Memphis, TN 38103, USA.

[4]Department of Pathology, Tohoku University Graduate School of Medicine, Sendai, Miyagi 980-8577, Japan.

[5]Molecular Bioinformatics Core, University of Tennessee Health Science Center, Memphis, TN 38103, USA.

[6]Department of Pathology, College of Medicine, University of Tennessee Health Science Center, Memphis, TN 38103, USA.

[7]West Cancer Center and Research Institute, Memphis, TN 38138, USA.

[8]Department of Ophthalmology, College of Medicine, University of Tennessee Health Science Center, Memphis, TN 38103, USA.

[9]Department of Pathology, Methodist Hospital, Memphis, TN 38104, USA.

[*]Corresponding author and lead contact: Dr. Ramesh Narayanan, Department of Medicine, Division of Hematology and Oncology, University of Tennessee Health Science Center (UTHSC), Cancer Research Building, 19 S. Manassas, Room 120, Memphis, TN-38103, Phone 901-448-2403, Fax. 901-448-3910, RNARAYA4@UTHSC.EDU.

Author contributions:

RN provided the overall supervision to the project. SA, ZY, HS, LMP, DDM, and RN contributed to conceptualization of different parts of the project. SA, WE, KLY, SP, TT, KM, YW, TH, and YK contributed to experiment design and/or experimentation. DJH, YH, BG, MDF, FEP, and AH provided critical resources for the project. JH, LC, DJ, BG, ZY, FK, LM, DNH, and MF contributed to data analysis. RN and SA wrote the manuscript and remaining authors reviewed and edited the manuscript to generate the final version.

Competing interests: RN is a consultant to Oncternal therapeutics. The selective androgen receptor degraders (SARDs) mentioned in this manuscript are licensed to Oncternal therapeutics Inc., San Diego, CA by the University of Tennessee Research Foundation (UTRF) under an exclusive licensing agreement. SP, DJH, YH, DDM, and RN are co-inventors in patents related to UT-105 and receive royalties.

[10]UTHSC Center for Cancer Research, University of Tennessee Health Science Center, Memphis, TN 38103, USA.

[11]Biomedical and Informatics Services Core, Houston Methodist Research Institute, Houston, TX 77030 USA.

Abstract

Triple-negative breast cancer (TNBC) is an aggressive subtype with no targeted therapeutics. The luminal androgen receptor (LAR) subtype constitutes 15% of TNBC and is enriched for AR and AR-target genes. Here, we show that a cohort of TNBC not only expresses AR at much higher rate (~80%), but also expresses AR splice variants (AR-SVs) (~20%), further subclassifying LAR-TNBC. Higher AR and AR-SV expression and corresponding aggressive phenotypes are observed predominantly in specimens obtained from African American women. LAR TNBC specimens are enriched for interferon, JAK-STAT, and androgen signaling pathways, which are exclusive to AR-expressing epithelial cancer cells. AR and AR-SV-expressing TNBC cell proliferation, xenograft and patient-tumor explants growth are inhibited by AR N-terminal domain (NTD)-binding selective AR degrader (SARD) or by a JAK inhibitor. Biochemical analysis suggests that STAT1 is an AR coactivator. Collectively, our work identifies pharmacologically targetable TNBC subtypes and identifies growth-promoting interaction between AR and JAK-STAT signaling.

Keywords

Triple-negative breast cancer (TNBC); Luminal androgen receptor TNBC (LAR TNBC); androgen receptor (AR); AR splice variant (AR-SV); AR-V7; Selective AR degrader (SARD); JAK STAT pathway; ruxolitinib; coactivator

INTRODUCTION

Breast cancer (BC) is the second leading cause of cancer-related death in women[1]. Approximately 30% of all cancers diagnosed in women are BC and 15% of those women will die of this cancer[1]. Though the mortality rate from BC has decreased, the incidence continues to increase[1]. BC is classified into hormone receptor positive (HR-positive), HER2-positive, and triple-negative (TNBC)[2], with TNBC accounting for about 15% of BC[3]. TNBC is more prevalent in younger women and in women of African descent[4–6]. TNBC is a heterogeneous disease that lacks molecular targets, and hence challenging to treat[4–6]. TNBC tumors are usually aggressive, larger in size, present with a higher grade, have lymph node involvement at diagnosis, and a higher frequency of distant metastasis[4–6]. Patients with TNBC have poorer prognosis and have fewer treatment options than patients diagnosed with other BC[3].

TNBC is divided into six molecular subtypes: basal-like 1 and 2 (BL1 and BL2), immunomodulatory (IM), mesenchymal (M), mesenchymal stem–like (MSL), and luminal androgen receptor (LAR)[4]. LAR TNBC is a differentiated subtype that expresses AR mRNA, protein, and AR downstream targets and coactivators[4]. Approximately 15% of TNBC is classified into LAR subtype, though this number varies significantly between studies[4, 7–9]. The LAR subtype typically has a lower pathological grade and is commonly

diagnosed in older women[4, 7]. Unfortunately, these tumors respond to neoadjuvant chemotherapy at lower rates when compared to other TNBC subtypes[7, 10]. Recent studies have shown that AR is targetable in TNBC and AR antagonists, enzalutamide, bicalutamide, and androgen synthesizing enzyme inhibitor, abiraterone were tested clinically to treat this subtype[11–14].

AR is a member of the hormone receptor family of ligand-activated transcription factors[15–17]. AR has a modular structure with a N-terminal domain (NTD), DNA-binding domain (DBD), a hinge region, and a ligand-binding domain (LBD)[15–17] (Fig. 1A). The NTD comprises of an activation function-1 (AF-1) domain that retains over 70% of AR's transcriptional function[15–17]. The LBD expresses eleven helices and contains the AF-2[18]. AF-1 is the primary cofactor-interacting domain of the AR[15–17].

LAR TNBC has similarity to prostate cancer (PCa), which is also dependent on AR for its growth[19]. Studies have suggested that AR antagonist-resistant castration-resistant PCa (CRPC) has AR amplification and expression of LBD-null AR splice variants (AR-SVs)[18–21] (Fig. 1A). Patients with CRPC expressing AR-V7 (predominant clinical AR-SV isoform), exhibit a more aggressive disease with shorter progression-free and overall survival rates[21–23]. AR-SV-positive CRPCs do not respond to any currently FDA-approved targeted-therapeutics, making them one of the most difficult subtypes to treat[24–26]. Interestingly, AR-SVs have also been shown to be expressed in breast cancer cell lines and patient specimens[27, 28]. Similar to CRPC, treatment of patients with LAR TNBC with AR antagonist enzalutamide and a PI3K inhibitor resulted in an increase in AR-V7 expression, which was associated with a lack of response[28]. The presence of AR-SVs in LAR TNBC could make LBD-binding competitive AR antagonists less effective in patients with TNBC[11, 21, 28–30]. To overcome this potential resistance due to AR-SVs, our group and others have discovered molecules that bind to non-canonical AR domains such as the NTD and DBD (Fig. 1A)[29, 31–39].

Recently, one of the important signaling pathways shown to be critical in PCa and that drives lineage plasticity is Janus kinase (JAK)-signal activator and transducers (STAT)[40, 41]. The JAK-STAT pathway is activated by cytokines, interferons, and other signaling molecules, and inhibiting JAK-STAT reduces proliferation of resistant PCa cells and tumors[40–44]. The role of interferon and JAK-STAT signaling in breast cancer, especially in LAR TNBC, nor on AR function is unclear.

In this study, we show that LAR TNBC expresses AR at a higher rate than was originally reported and also expresses AR-SVs. Both AR and AR-SV expression is higher in African American (AA) women and drive aggressive growth. LAR and LAR AR-SV specimens from patients with TNBC are enriched for JAK-STAT signaling pathway with STAT1 functioning as a coactivator of AR and driver of TNBC growth. LAR TNBC cell line-derived xenograft (CDX) and LAR-AR-SV TNBC patient-derived xenograft (PDX) tumor growth respond to small molecule selective AR degrader (SARD) UT-105 that inhibits both AR and AR-SV, but not to canonical LBD-binding AR antagonists[29, 31, 45].

RESULTS

Patients with TNBC express full-length AR and AR-SVs

The prognosis of patients with LAR TNBC expressing AR was evaluated using the KM plotter tool[46]. The samples were split at median expression and the ER, PR, and HER2 negativity was defined by immunohistochemistry. All PAM50 subtypes were included in the analysis. Patients expressing higher AR have worse relapse-free survival (RFS), compared to those expressing lower levels of AR (Fig. 1B). The hazard ratio of AR high group was 1.37, indicating a 37% increase in probability of a relapse. The difference in RFS was statistically significant. The lower AR expressing cohorts had a survival of 36.84 months, while the higher AR expressing patients had a survival of 27.34 months. Previous studies have shown that only 10–15% of patients with TNBC express AR and could be classified as LAR subtype[4]. However, these studies were predominantly comprised of Caucasian American (CA) women. Considering that AA women suffer from some of the most aggressive forms of breast cancer[47, 48], we hypothesized that they may have a higher proportion of the complex subtype such as LAR TNBC. A small set of specimens from patients with TNBC from AA women was screened for AR expression at the protein level using an antibody that binds to the AR-NTD. Interestingly, these patients expressed AR forms at molecular weights that were distinct from AR and that corresponds to the size of AR-SVs (Fig. S1A). To determine the AR expression in a large patient cohort, 52 specimens from TNBC patients were prospectively collected and evaluated for the expression of AR wherein the majority of patients were AA (Fig. 1C). Real-time PCR (RT-PCR) probes that bind to the AR NTD were used to obtain a snapshot of AR and AR-SV expression in patient specimens (Fig. 1D). AR expression was almost 4-fold higher in AA women compared to CA women. AR expression was determined at the protein level using immunohistochemistry (IHC) using a cutoff of 10% (number of cells and intensity of staining). Interestingly, 42 of the 52 patients (81.25%) expressed AR at the protein level with AA women expressing higher AR than CA women, though not statistically significant (Fig. 1E and S1B). Surprisingly, unlike the previously reported 15–40% AR expression, more than 80% of the patients in our cohort express AR[49, 50]. This is in agreement with an enzalutamide clinical trial where over 60% of specimens from TNBC patients were positive for AR[11].

We then adopted a method to determine AR-SVs in our cohort using TaqMan probes that specifically bind to the LBD and NTD. Since AR-V7 is only one of the several AR-SVs[19, 29], higher signal with NTD probe relative to the LBD probe was interpreted as expression of AR and an AR-SV (Fig. 1F and S1C). This approach is similar to the work previously published in PCa[51, 52]. As expected, RNA from AR-positive LNCaP PCa exhibited a ratio of 1, while AR- and AR-SV-positive 22RV1 PCa cells exhibited a ratio of greater than 1. A subset of patients (12/52; ~23%) expressed some variant of AR as shown by an NTD/LBD ratio of greater than 1.5 (Fig. 1F). All specimens, except one, that had a ratio of greater than 1.5 were obtained from AA women.

Since AR-V7 is the most expressed AR-SV in CRPC[19, 29], AR-V7 mRNA expression was quantified by RT-PCR (Fig. 1G). AR-V7 expression was confirmed using IHC and gene expression (Fig. S1D). Although only 12% of patients expressed AR-V7, the NTD/LBD

ratio of greater than 1.5 in a larger subset of specimens suggests that other AR-SVs are expressed besides AR-V7. Interestingly, all patients expressing AR-V7 were AA women. Collectively, these studies make this subset a LAR-AR-SV TNBC subtype (Fig. 1H).

AR-SV expression results in a more aggressive disease type

Since this is only the second documentation of AR-SV expression in specimens from TNBC patients, its role in TNBC is unknown and not well evaluated[28]. We hypothesized that AR-SVs cause a more aggressive phenotype in TNBC, similar to their action in CRPC[29]. AR-V7 was stably transfected (lentivirus[53]) into AR-positive TNBC cell lines, MDA-MB-453, BT549, and MFM223, and an AR-negative MDA-MB-231 cell line (figures S2A–D). MDA-MB-453 is one of the most widely used models to study LAR TNBC, where AR is the driver oncogene of its proliferation[4, 54]. AR-V7 significantly increased the proliferation in three out of four cell lines (Fig. 2A) and migration compared to AR-FL-expressing control lines (Fig. 2B). To confirm the increased proliferative properties of AR-SVs, TNBC specimens were separated into AR-positive and AR and AR-SV -positive, and Ki67 staining was performed. Patient specimens that express AR-SV had higher Ki67 (Fig. 2C).

To determine the effect of AR-SV on global transcriptome, RNA-sequencing was performed in LAR TNBC cells (MDA-MB-453 (453) and MDA-MB-453-AR-V7 (453-V7)) and AR+/AR-SV+ve patient specimens. Gene set enrichment analysis (GSEA) showed enrichment in mitotic spindle, G2M checkpoint, and E2F Hallmark pathways in 453-V7 and AR+/AR-SV+ patient specimens when compared to controls (453 and AR+ patient specimens as controls, respectively) (Fig. 2D–E; 2E left panel (MDA-MB-453 vs 453-V7 FDR>0.25; not significant). The E2F pathway has been correlated with tumor progression, angiogenesis, and metastasis[55, 56]. These studies show that AR-SVs may play an important role in causing more aggressive disease in patients with LAR TNBC.

SARD UT-105 is an irreversible AR antagonist.

Modest efficacy with AR-LBD-binding competitive antagonists in TNBC clinical trials[11, 12] supports the need to discover novel interventions. In tumors from patients with TNBC that express AR and AR-SV, an LBD-binding competitive antagonist will likely only inhibit AR-FL, but not AR-SVs[21]. To test the possibility that an AR NTD-binding SARD could be effective in LAR TNBC models, SARDs developed in our laboratory were used[29, 31, 34–37]. These SARDs degrade AR and AR-SVs by binding to the NTD[29, 31].

From our SARDs library we chose UT-105 (Fig. 3A) for further characterization. UT-105 selectively inhibited wildtype and enzalutamide-resistant mutant AR transactivation[57] (Fig. 3B). UT-105 was selective to AR as it failed to inhibit the transactivation of glucocorticoid (GR) or mineralocorticoid (MR) receptors (Fig. S3A). UT-105 minimally cross-reacted when tested in a panel of kinases (468) and 168 GPCRs (Fig S3B).

UT-105 downregulated AR expression, similar to other molecules belonging to this scaffold[29, 31] (Fig. 3C). We expected that the effect of UT-105 is due to its binding to AR NTD, due to our prior experience with molecules belonging to this scaffold[29, 31]. We used a SYPRO Orange assay to test UT-105 binding to AR NTD. Real-time PCR with rising temperature revealed SYPRO Orange binding to lipophilic amino acids in UT-105-

bound AR NTD. Protein heating caused melting, enabling SYPRO Orange to bind to these amino acids. Disordered proteins lack a melt curve, but transitioning from disorder to order produces a melt curve[58, 59](Fig. 3D). One of the characteristics of intrinsically disordered proteins is the temperature-dependent instability[34, 60]. Binding of small molecules to a protein will change the protein conformation, resulting in an increase in the protein's stability[61, 62]. AF-1 and AR-V7 purified recombinant proteins when incubated with vehicle for 4 hours at room temperature was barely visible due to rapid destabilization at room temperature. However, when the proteins were incubated with UT-105 or another SARD molecule, UT-34[31], both AF-1 and AR-V7 stabilized. This result further established the binding of UT-105 to AR NTD that results in a potential change in conformation (Fig 3D lower panel; Fig. 3E). Competitive ligand-binding assay with purified AR LBD recombinant protein showed no binding of UT-105 to LBD, unlike DHT, suggesting that UT-105's AR inhibitory properties are due to its binding to AR NTD (Fig. S3C).

Considering the structural characteristics of UT-105 to our covalent molecules[35], we evaluated UT-105 in a Schild plot[34]. A reversible inhibitor typically increases the EC_{50} of an agonist, while an irreversible inhibitor inhibits the E_{max} of the agonist in a transactivation assay. While UT-105 inhibited the Emax, enzalutamide only increased the EC_{50} of R1881, but failed to inhibit the E_{max}[34] (Fig. 3F and S3D), suggesting that UT-105 may have a distinct dual mechanism of action (irreversible inhibition and degradation).

UT-105 potently inhibits AR function in TNBC cell line models

R1881-stimulated expression of AR-target genes *FKBP5*, *STEAP4*, and *TMPRSS2* was inhibited by enzalutamide and UT-105 (Fig. 3G). UT-105 inhibited the expression of *TMPRSS2* to a level below that of the vehicle. To determine the effect of UT-105 on androgen-dependent global gene expression, RNA from MDA-MB-453 cells treated with UT-105 or vehicle in the presence of R1881 was sequenced and the data were analyzed using GSEA (Fig 3H). With an FDR of 0.05 and a fold change cut off of 1.5, UT-105 differentially regulated the expression of 3964 genes, with 1127 down-regulated and 2837 up-regulated. Expression of androgen-responsive genes such as *FKBP5*, *NDRG1*, *SGK1*, *AQP3*[63], *S100P*[64], and others were reversed by UT-105. Some of the UT-105 up-regulated genes include *IGFBP3*[65], *MGP*[66, 67], *PRKD1*[68] that are all androgen repressed genes.

UT-105 inhibited R1881-induced proliferation of AR-dependent MDA-MB-453 cells, but not AR-negative MDA-MB-231 cells, demonstrating selectivity to AR-expressing cells (Fig. 3I and S3E). Unlike LBD-binding antagonists[19, 29, 31, 69] UT-105 inhibited the colony formation of AR-V7-expressing cells (Fig. 3J). These effects were not observed in AR-negative MDA-MB-231 TNBC cells (Fig. S3F), AR-negative PC-3 PCa cells (Fig S3G) and PC-3 tumor xenograft (Fig S3H). Collectively, these data suggest that the UT-105 effectively degrades AR, irreversibly inhibits AR, inhibits AR-target genes, and significantly inhibits proliferation and colony formation in cells expressing AR and AR-V7, warranting further evaluation in LAR and LAR AR-SV TNBCs.

Considering that AR-V7 was ectopically expressed, we ensured that it functions comparably to intrinsically expressed AR-V7. We performed Chromatin immunoprecipitation (ChIP)-PCR to determine AR-V7 recruitment to androgen response elements (ARE) of AR target

genes and the effect of UT-105 on this recruitment (Fig. S3I). AR-V7 was recruited to the ARE in *FKBP5* regulatory region and this recruitment was inhibited by UT-105, similar to other molecules belonging to the scaffold[29, 31]. This result suggests that the ectopically expressed AR-V7 is recruited to ARE similar to endogenous AR-V7, and that UT-105 inhibits this recruitment.

UT-105 exhibits drug-like properties.

A pharmacokinetic (PK) assay of UT-105 in rats showed that UT-105 was well absorbed and exhibited low clearance, high area under the curve, and long half-life, with $t_{1/2}$ undetermined due to 50% of the drug not metabolized after 24 hours (Fig. S4A). A pharmacodynamic (PD) Hershberger assay where male rats were treated for 13 days showed that UT-105 reduced androgen-dependent seminal vesicles weight to the level of surgical castration with an IC_{50} of less of 1 mg/kg/day (Fig. S4B). UT-105 had extremely low plasma protein binding of 65–70% (Fig. S4C), suggesting high free drug availability to act. UT-105 also did not inhibit hERG channel that is indicative of cardio safety (Fig. S4D) and had minimum cytochrome P450 inhibition (Fig. S4E) that suggests a minimum drug-drug interaction liability.

UT-105 potently inhibits TNBC tumor growth.

To test the effect of UT-105 in vivo, xenograft studies were performed in an orthotopic TNBC model (Fig. 4A). UT-105, but not enzalutamide and bicalutamide, inhibited the MDA-MB-453 tumor growth with a tumor growth inhibition (TGI) of >90% (Fig. 4B). UT-105 had no effect on body weight of tumor-bearing mice (Fig. 4C). Enzalutamide and bicalutamide doses were selected based on our previous publications in PCa tumor xenografts and pharmacodynamic models[29, 70]. Earlier studies have shown that enzalutamide inhibits MDA-MB-453 xenograft growth. However, those studies were conducted with MDA-MB-453 implanted in female mice supplemented with DHT[71], while our studies were conducted in female mice without supplementation. Hence, the tumor growth in this study was spontaneous due to intra-tumoral androgens that is comparable to patients' tumor environment.

We also tested the effects of UT-105 on a LAR TNBC PDX model, UT-1355 that was developed from one of the patient specimens shown in Fig. 1C. This PDX expresses AR-FL and AR-V7 (Fig. 4D–4E), making it an appropriate model to evaluate UT-105. While UT-105 potently inhibited the growth of UT-1355 PDX with a TGI of >90% with no effect on body weight, enzalutamide was modestly effective (Fig. 4F, 4G). UT-105 significantly reduced tumor weights compared to vehicle and enzalutamide in the PDX model (Fig. 4H). Thus, LAR TNBCs expressing AR or AR and AR-SV can be effectively treated with an NTD-binding SARD, like UT-105.

UT-105 inhibits JAK-STAT signaling enriched in LAR and LAR-AR-SV TNBC

RNA-sequencing was performed in the tumors obtained from the MDA-MB-453 xenograft tissues to define underlying SARD-specific mechanisms in reducing tumor burden compared to canonical AR antagonist, enzalutamide. UT-105-treated tumors differentially expressed 291 genes, while enzalutamide-treated tumors only differentially expressed eight (Fig.

5A). GSEA analysis found that the HALLMARK_INTERFERON_ALPHA_RESPONSE, HALLMARK_INTERFERON_GAMMA_RESPONSE, and HALLMARK_IL6_JAK_STAT3_SIGNALING pathways were all significantly downregulated (FDR < 0.25) by UT-105 compared to vehicle-treated tumors (Fig. 5B–C). In addition to the JAK-STAT pathway, HALLMARK_ANDROGEN_RESPONSE, EARLY_ESTROGEN_RESPONSE, AND LATE_ESTROGEN_RESPONSE pathways were also observed in the GSEA analysis, though the FDR was above the cutoff of 0.25. Since the androgen response pathway was not significantly altered in the GSEA analysis, we took a different approach to characterize the regulation of the androgen pathway by UT-105. We merged the 291 differentially regulated genes in UT-105-treated tumors with androgen response element (ARE) list obtained from Wilson et al.[72]. Approximately two-thirds (197/291) of the UT-105-regulated genes aligned with the genes that express ARE in their regulatory region. This indicates that androgen response pathway genes are highly regulated by UT-105. The list of upstream ARE-coding genes expressed in our dataset is provided in the supplement table ST3.

Previous studies have shown that type I and type II interferon (IFN) response pathways have significant overlap[58, 73, 74]. The expression of interferon-stimulated genes (ISGs), including IFN response factors (IRFs) that further drive the transcription of effector genes[75], was assessed in the RNA-seq data. UT-105 effectively reduced IRF1, IRF7, and IRF9 expression in tumors (Fig. 5D). Expression of a select list of chemokines decreased in UT-105-treated tumors, confirming the effect on downstream pathways (Fig. 5E). UT-105 also inhibited the phosphorylation of STAT1, STAT3, and AKT in MDA-MB-453 tumors (Fig. 5F). These proteins are important components of the JAK-STAT signaling pathway[73].

Since UT-105 inhibited STAT1 phosphorylation in MDA-MB-453 tumors that were treated for 28 days, it is unclear if UT-105 will have an effect on STAT1 phosphorylation when treated for a short duration. To evaluate this surmise, MDA-MB-453 cells were pretreated for 24 hours with ruxolitinib or UT-105 followed by induction of STAT1 phosphorylation by interferon-α for 30 minutes (Fig 5G). While ruxolitinib completely inhibited the phosphorylation of STAT1, UT-105 only marginally inhibited the STAT1 phosphorylation, suggesting that complete inhibition of STAT1 by UT-105 requires sustained treatment and the effect observed in the xenograft could potentially be the consequence of an indirect effect on the JAK-STAT pathway through AR.

To determine the importance of the JAK-STAT pathway for the proliferation of AR-SV-positive TNBC cell line growth, the JAK1/2 inhibitor ruxolitinib[76, 77] was used. MDA-MB-453 and MDA-MB-453-AR-V7 cells were treated with vehicle control, UT-105, ruxolitinib, or a combination of UT-105 and ruxolitinib (Fig. 5H). UT-105 inhibited proliferation of the parental and AR-V7-expressing TNBC cells, while ruxolitinib also rendered a comparable inhibition of cell proliferation. The combination of UT-105 and ruxolitinib did not lead to additional growth arrest, suggesting a potential crosstalk/overlap between AR and the JAK-STAT pathways.

Considering that MDA-MB-453 tumors and cells have enriched JAK-STAT pathway that were inhibited by UT-105 and JAK inhibitor ruxolitinib, we examined whether

tumors from LAR and LAR AR-SV patients are enriched for JAK-STAT pathway. We performed RNA sequencing with RNA extracted from the 41 patient specimens (though RNA was extracted from all 52 specimens shown in Fig. 1C and sequenced, sequence from only 41 specimens met the quality control for further analysis) shown in Fig. 1 and compared the gene expression of AR and AR-SV -positive specimens to AR-negative patient specimens. GSEA pathway analysis showed significant enrichment of hallmark signaling belonging to HALLMARK_IL2_STAT5, HALMMARK_IL6_JAK_STAT3, HALLMARK_INFLAMMATROY_RESPONSE, and HALLMARK_INTERFERON_GAMMA_RESPONSE (Fig. 5I–5J). One of the significantly enriched pathways in the AR+/AR-SV+ patient specimens is the HALLMARK_ANDROGEN_RESPONSE pathway, providing a validation of our real-time PCR and IHC data shown in Fig. 1 and the appropriate classification of these specimens as AR and AR-SV -positive specimens.

Spatial transcriptomics suggest that AR-positive epithelial cancer cells are enriched for JAK-STAT pathway and macrophage and stem cells.

Since majority of sequencing data on LAR TNBC are bulk sequencing, it is unclear how AR-expressing TNBC cells differ from AR-negative cells in a tumor microenvironment and how AR -positive cells contribute to the aggressive tumor growth in LAR TNBC. To clarify the role of AR at molecular level, we employed spatial transcriptomics (Nanostring, GeoMx; Fig. 6A). Three formalin-fixed paraffin-embedded patient specimens were stained for AR and panCK (cancer epithelial marker)[78, 79]. Cancer cells expressing high and low AR were captured (region of interest for a representative specimen shown in Fig. 6B) and sequenced (500 cells/cell type/patient specimen). Pair-wise statistical analysis showed that genes up-regulated in AR-high cancer cells compared to AR-low cells in the three specimens were enriched in pathways corresponding to stemness, epithelial-mesenchymal transition, stem cell transition, androgen signaling, and interferon-alpha and gamma pathways (Fig. 6C and 6D). These results clearly demonstrate that AR expression in a TNBC microenvironment contributes to the aggressive tumor phenotype and switches to a more stem cell phenotype. The enrichment of JAK-STAT signaling in AR high cells corroborate the findings made in preclinical models. This evidence in LAR TNBC shows how AR-expressing cells contribute to the tumor microenvironment.

STAT1 is an AR coactivator.

Enrichment of JAK-STAT pathway led us to hypothesize that this pathway crosstalks with AR and may be the driver of the oncogenic function of AR in LAR TNBC. Crosstalk between these two pathways is important for lineage plasticity in advanced PCa, an androgen-dependent disease[40, 41]. To examine the crosstalk between these pathways, we evaluated AR transactivation in the presence and absence of STAT1. The GRE-LUC reporter used in this study contains three Glucocorticoid response element (GRE) repeats that is the consensus binding site for AR, GR, PR, and MR. STAT1 significantly increased the R1881-induced AR transactivation (Fig. 7A). As GRE-LUC contains no STAT binding region, the effect is likely from the complex formation between AR and STAT1.

For a protein to be defined as an AR coactivator, it must interact with AR, recruited to the AREs, and increase AR's activity. Thus, we evaluated the interaction between AR and STAT1 by performing a co-immunoprecipitation assay. HEK-293 cells were transfected with AR and STAT1 and immunoprecipitated with IgG or AR antibody (Fig. 7B). Immunoprecipitation with AR antibody, but not IgG antibody, and Western blot for STAT1 clearly showed a robust interaction between AR and STAT1 (Fig. 7B). This interaction observed with ectopically expressed AR and STAT1 was confirmed with a colocalization experiment in endogenously expressing MDA-MB-453 cells using confocal microscopy (Fig. 7C). MDA-MB-453 cells were treated with interferon and R1881, and the immunostained AR and STAT1 were visualized using a confocal microscope. The results show that STAT1 and AR colocalize and interact in MDA-MB-453 cells. We then performed a ChIP PCR in MDA-MB-453 cells treated with interferon α and R1881. STAT1 was immunoprecipitated and PCR was performed for STAT1-response elements at *CXCL11* promoter, hIL8 promoter, and ARE in *FKBP5* regulatory region (Fig. 7D). STAT1 was recruited to the AREs at *FKBP5* upstream region and to the STAT1-REs at the *CXCL11* and *IL8* promoters. These results furnish evidence that STAT1 is an AR coactivator and provide a potential mechanism by which it increases the AR's oncogenic potential.

To determine if STAT1 interaction with AR leads to AR's recruitment to STAT-responsive genes regulatory regions, IgV tracks of AR ChIP-seq in PCa cells (22RV1) was utilized. The tracks show AR binding to *CXCL8* (*IL8*) regulatory region, which is a STAT1-responsive gene, and to *FKBP5* regulatory region, an androgen-responsive gene, which was used as a positive control (Fig. 7E). These results show that both STAT1 and AR interact and mutually recruit to their respective responsive gene regulatory regions. Since UT-105 robustly inhibits interferon JAK-STAT pathway through AR, we examined whether UT-105 influenced STAT recruitment to its response element and to AREs by performing ChIP assays with STAT1 antibody in MDA-MB-453 cells treated with UT-105. The experiment was also performed to determine if STAT1 recruitment to the DNA requires coincubation of interferon and R1881. MDA-MB-453 cells treated with either R1881 or interferon recruited STAT1 to STAT1RE and ARE, showing that coincubation with interferon and R1881 is not required to promote recruitment of STAT1 to the DNA (Fig. 7F). Although interferon robustly recruited STAT1 to STAT1RE, the magnitude of this recruitment was reduced by R1881, which could potentially be due to a potential sequestration of STAT1 from STAT1RE to ARE. This recruitment of STAT1 to the DNA was inhibited by UT-105 (Fig. 7F).

Since STAT1 collaborates with AR and drives AR function and LAR TNBC growth, we evaluated the effect of inhibiting STAT1 with ruxolitinib on AR function. MDA-MB-453 cells were maintained in charcoal-stripped serum-containing medium for two days and treated with 0.1 nM R1881 alone or in the presence of ruxolitinib. Twenty-four hours after treatment, the cells were harvested, RNA extracted, and real-time PCR for androgen-dependent gene, *FKBP5* was performed. R1881-induced expression of *FKBP5* was completely inhibited by ruxolitinib, suggesting that STAT1 is important for AR function in LAR TNBC (Fig 7G).

We performed AR transactivation in the presence or absence of STAT1 to evaluate the effect of UT-105 in breaking this STAT1 driven AR activity. Enzalutamide increased the EC_{50}

of R1881 in the presence or absence of STAT1 but had no effect on the E_{max} of R1881. Ruxolitinib had no effect on R1881-dependent AR transactivation in the absence of STAT1 but inhibited STAT1-dependent increase in AR transactivation, confirming that ruxolitinib is selective to JAK-STAT pathway, and lacks the ability to inhibit basal AR transactivation (Fig. 7H). Interestingly, UT-105 (Fig. 3F), inhibited AR transactivation significantly in the presence and absence of STAT1. UT-105 inhibited the EC_{50} and the E_{max} of R1881 significantly to a level below that of the STAT1 independent AR transactivation (Fig. 7H).

To validate the findings in a more clinically relevant setting, patient specimen explants were cultured in 3-dimentional culture (on dental sponges) and were treated with ruxolitinib and UT-105 for 48 hours and stained for ki67 (Fig. 7I). Tissues treated with UT-105 and ruxolitinib (one out of two) had decreased Ki67 staining (Fig. 7I). These results suggest that an irreversible inhibitor of AR and an AR degrader that is capable of blocking STAT-dependent AR activation has the potential to inhibit the LAR TNBC growth.

DISCUSSION

The results presented in this manuscript provide critical molecular and biological insight into the LAR TNBC subtype. First, we identified a class within the LAR subtype, LAR-AR-SV, which exhibits aggressive growth and migration, and fails to respond to canonical AR antagonists, enzalutamide and bicalutamide, but responds to SARDs. This observation was previously reported in a clinical trial where a small subset of patients expressed AR-SV and this expression increased upon treatment with AR antagonist, enzalutamide[28]. In that trial, enzalutamide alone or in combination with PI3K inhibitor taselisib failed to have an effect in patients expressing AR-V7 and the expression increased in some patients at the end of the trial, compared to pre-treatment. This result suggests that similar to CRPC, LAR TNBC needs new treatment modality like our SARD, UT-105 that could inhibit both the AR and AR-SV. Our results corroborate the findings made in the clinical trial. Also, spatial transcriptomics experiment defines the aggressive stem-like phenotype of AR-positive cells in LAR TNBC tumor microenvironment. Finally, we provide clear evidence that STAT1 is an AR coactivator that is inhibited by UT-105, rendering further evidence for the therapeutic efficacy of UT-105 in LAR TNBC.

Although the LAR subtype was previously estimated to only occur in about 15% of patients with TNBC[4], here we show that AR and AR-SV are highly prevalent in specimens from TNBC patients. Similar to PCa, LAR TNBC is driven by AR expression[4, 18]. Most interestingly, we have shown that TNBC expresses AR-SVs and that AA women have higher expression of AR-SVs. We demonstrate that ectopic expression of the most common AR-SV, AR-V7, in multiple TNBC models contributes to more aggressive disease, like PCa[19, 29]. In patients with LAR TNBC, AR-SV showed a correlation with higher tumor cell proliferation and an enrichment of proliferation related pathways, especially E2F[56]. The E2F pathway is associated with tumor progression and metastasis in breast cancer[56].

Canonical AR antagonists such as enzalutamide and bicalutamide, which bind to the LBD, though effective in preclinical models have not shown convincing efficacy in clinical trials[11, 12]. Therefore, there is a critical need to develop AR antagonist that target non-canonical

domains, such as the NTD, to treat TNBC and other AR-dependent cancers. SARDs bind to the NTD and effectively degrade AR and AR-SV in preclinical models of PCa and CRPC[29, 31, 37]. Activated JAK-STAT signaling upregulates the expression of interferon-stimulated genes (ISGs) and the release of chemokines[75, 80, 81]. JAK-STAT signaling also stimulates the STAT1-PI3K-AKT axis that activates the mammalian target of rapamycin (mTOR) pathway[75, 80–83]. Future studies should investigate whether AR expression is increased in TNBC as a result of JAK-STAT activation and whether treatment with JAK1/2 inhibitors and SARDs can revert TNBC to a less aggressive state. The discovery that STAT1 is a coactivator of AR adds to the lists of over 200 AR coactivators already discovered. It is unknown whether the AR-STAT1 interaction occurs in LAR TNBC and in CRPC. We have summarized the findings as a model, shown in figure 7J.

Collectively, SARDs degrade AR protein and cause cytostasis through JAK-STAT pathway inhibition in LAR and LAR-SV TNBC subtypes. Expression of AR-SVs cause more aggressive disease, which is inhibited by SARDs treatment. Future clinical trials will provide translational significance of using a SARD and/or a JAK/STAT pathway inhibitor for the treatment of LAR and LAR-AR-SV TNBC.

Limitations of the study.

The previously unreported coactivator role of STAT1 in the context of AR function is a notable finding of this study. However, it is essential to acknowledge certain limitations. Firstly, the lack of clinical validation for the involvement of STAT1 in this coactivation and its impact on the growth of LAR TNBC is a constraint. Secondly, our identification of the LAR-AR-SV subtype was based on a relatively small sample size of n=52 specimens. To enhance the robustness and generalizability of these findings, a validation cohort should be considered in future research efforts. Thirdly, the absence of endogenously expressing AR and AR-SV-positive TNBC cell line models present another limitation. This challenge can be addressed by either screening multiple cell lines or by establishing a cell line derived from our PDX model, UT-1355. These steps are crucial to further investigate the role of STAT1 in AR-mediated signaling pathways in TNBC.

STAR Methods

Resource availability

Lead contact—Dr. Ramesh Narayanan

rnaraya4@uthsc.edu

Materials availability—UT-105 can be obtained from Oncternal therapeutics, licensee of the program from the university of Tennessee research foundation (UTRF). This was generated in our laboratory

Data and code availability

- All the RNA sequencing data are deposited in GEO database (https://www.ncbi.nlm.nih.gov/geo/) and the accession numbers are provided in the table above.
- Any additional information required can be directed to the lead contact.
- No codes were generated in the manuscript.

Experimental model and study participant details

Cell culture—LNCaP, 22RV1, MDA-MB-453, MDA-MB-231, and BT549 cells were obtained from American Type Culture Collection (ATCC, Manassas, VA). MFM223 cells were obtained from Sigma Aldrich (St. Louis, MO). The cells were cultured according to ATCC recommendation and were authenticated by short terminal DNA repeat assay (Genetica cell line testing laboratory). Cells were also frequently tested for mycoplasma.

Clinical patient specimens—Specimens from patients with breast cancer were collected with patient consent under a protocol (14–03113XP) approved by the UTHSC Institutional Review Board (IRB). Patient characteristics are provided in figure 1C and supplementary table ST1. Specimens were collected immediately after surgery. One piece of tumor tissue was placed in RPMI medium containing penicillin:streptomycin and Fungizone and a piece was snap frozen in dry ice. The tumors were transported to the laboratory on ice or dry ice. Tissues were finely minced and frozen in liquid nitrogen in freezing medium (5% DMSO+95% fetal bovine serum (FBS)) or implanted under the mammary fat pad in female NSG mice to develop PDX models.

Method details

KM Plotter—The relapse-free survival of patients expressing high and low levels of AR (Affy ID: 211621_at) was evaluated in LAR TNBC according to Pietenpol subtype[4, 46]. Patients were split by the median.

Cell transfection—Viruses were made at the University of Tennessee Health Science Center (UTHSC) viral vector core laboratory[85, 86]. Cells were plated in six well plates in growth medium. Twenty-four hours after plating, the cells were infected with virus particles containing the AR-V7 plasmid mixed with polybrene. Cells were allowed to be infected for overnight, medium changed, and the cells were selected using puromycin. One week after selection, the cells were propagated, and the expression of AR-V7 was evaluated using Western blot.

Western blot—Tumors were homogenized in lysis buffer using a handheld homogenizer. Tumor fragments or cells were suspended in lysis buffer (50 mM Tris pH8, 137 mM NaCl, 1% glycerol, 1% NP40, 2 nM EDTA) containing protease and phosphatase inhibitors, and subjected to three freeze-thaw cycles. Protein concentrations were measured by BCA assay. Equal amounts of protein were fractionated on an SDS-PAGE and transferred to a PVDF membrane. Western blot was performed as previously described[70].

Sulforhodamine Blue Assay—Cells were plated in growth medium in 96 well plates. Cells were treated for the duration indicated, and medium was changed every third day. Cell viability was measured by sulforhodamine blue (SRB) assay.

Colony formation assay—Cells were plated in 6 well plates and treated for the duration indicated in the figures. Medium was changed every third day. Colonies were fixed with acetone and methanol solution. Cells were stained with crystal violet solution. Colonies were quantified using ImageJ software.

Scratch assay—Cells were plated in 6 well plates and after the cells attach to the plate overnight, a scratch was made using a pipette tip. Pictures of the wells were taken for the indicated duration on an Evos FL microscope (Life Technologies, Carlsbad, CA). The images were analyzed using ImageJ software.

BrdU assay—Cells were plated in 96-well plate in growth medium and were treated for the duration indicated. BrdU assay was performed on cells using Cell Signaling BrdU kit (Danvers, MA).

Gene expression assay—Cells were plated in 96 well plates in charcoal stripped serum-containing medium and maintained for two days. Medium was changed and then treated as indicated. RNA extraction and cDNA synthesis were performed using cells-to-ct kit (Thermo Fisher, Waltham, MA). Gene expression studies in tumors were performed by extracting RNA using RNA extraction kit from Qiagen (Hilden, Germany) and cDNA synthesized using High-Capacity RNA rt kit (ThermoFisher). Gene expression assays were performed using TaqMan real-time PCR primers and probes on Bio-Rad PCR machine. While most of the primers and probes used were Taqman primers and probes, AR-V7 primers and probe were custom made.

Tumor xenograft—Xenograft experiments were performed as previously published[70] according to a UTHSC Institutional Animal Care and Use Committee (IACUC) approved protocol. UT-1355 PDX was created using specimen collected from an African American patient according to an IRB approved protocol. UT-1355 PDX tumor fragments (1 mm^3) were surgically implanted under the mammary fat pad in female NOD SCID Gamma (NSG) mice (n=8–10/group). MDA-MB-453 5 million cells were implanted with Matrigel matrix (medium: Matrigel 1:1) under the mammary fat pad of female NSG mice. Once the tumors reach 100–300 mm^3, the animals were randomized and treated by oral gavage. Tumor volume was measured twice weekly, and body weight was measured at the start and end of the treatment period. At the end of the study, animals were sacrificed, and tumors were excised, weighed, and stored for further analyses.

Tumor volume was calculated (length * [width*width] * 0.5) and normalized to the measurement on the first day of treatment. Percent change was then calculated and then graphed. Linear regression was used to compare the lines for statistical significance.

RNA-seq assay—Integrity and quantity of RNA extracted from the tumors or cells were assessed using Agilent Bioanalyzer. Replicates from each group for cell lines and from

52 tumor specimens were submitted to Novogene (Cambridge, UK) or UTHSC molecular resources center for RNA-seq analysis.

Fastq files from Illumina HiSeq that passed quality control processing using FastQC (v0.11.8, table ST2) were first aligned to the human transcriptome (hg38 genome build, GENCODE v39 transcript annotation) using STAR (2.7.0, table ST2) and then sorted with SAMtools (v1.9, table ST2). Salmon (v0.13.1, table ST2) was then used for transcript quantification and gene level counts were used for data analysis in R version 4.1.2 (table ST2). Read counts were loaded from salmon quant files using tximport (v1.6.1, table ST2), and differential gene expression analysis between vehicle and treatment groups was performed using DESeq2 (1.28.1, table ST2). An adjusted p-value < 0.1 was used to determine significantly differentially expressed genes (DEGs) from each sample group described in the previous section. Read counts were normalized for downstream analyses and visualization using the regularized log transformation (rlog) from DESeq2. Heatmaps representing rlog normalized and scaled expression values were generated with the ComplexHeatmap package (v2.4.3, table ST2) where rows and/or columns were clustered via the “Pearson” distance method.

GSEA software was used (GSEA v4.2.3, www.gsea-msigdb.org/) to identify enriched gene signatures. GSEA analysis was performed by using rlog normalized gene expression data obtained from vehicle and treated tumors (n = 5, replicate n = 3). One thousand gene set permutations were used to test for significance using a false discover rate (FDR) cutoff of 0.25. The MSigDB hallmark gene sets (H collection) (v7.5.1, table ST2) were used to determine significantly enriched hallmark pathways in vehicle and treated groups.

Immunohistochemistry (IHC)—Fifty-two cases of TNBC formalin-fixed paraffin-embedded blocks (characteristics shown Fig. 1B) were sectioned at a thickness of 3 μm and mounted on glass slides. The slides were stained for AR and AR-V7 (AR, 1:50 dilution; AR-V7, 1:50 dilution) using IHC protocol previously described[70]. The slides were then analyzed by a trained and board-certified pathologist who was blind to the ID of the sections. The sections were digitally imaged using Image J. The color threshold function of Image J was used manually to define stromal areas on this photomicrograph and area as a percentage of total cellular area was calculated using the histogram function.

SYPRO Orange—SYPRO orange thermal shift assay was performed using the Bio-Rad kit and protocol (Hercules, CA).

Quantification and visualization of differential expression for AR and markers across three subgroups of patients with TNBC—For each of the three genes of interest, AR, WNT7A and TP63, Student’s t-test with Bonferroni correction was applied to compare the expression levels across AR-low, AR-mid and AR-high group. Matlab package Violin Plot (https://www.mathworks.com/matlabcentral/fileexchange/45134-violin-plot) was used to generate violin plots illustrating the distribution of gene expression levels amongst all the patients with TNBC within each subgroup.

Digital spatial profiling of Human Breast Carcinoma Tissue.—Paraformaldehyde-fixed, paraffin-embedded human breast cancer tissue was profiled using GeoMx® DSP (Merritt et al). Thin (5 μm) tissue sections were prepared according to manufacturer's recommendations for GeoMx-NGS RNA BOND RX Semi-Automated RNA Slide Preparation Protocol (FFPE) (manual no. MAN-10151–02). Following an overnight bake at 65°C, deparaffinization, rehydration, heat-induced epitope retrieval (for 10 minutes at 100°C with Bond Epitope Retrieval 2 Solution), and enzymatic digestion (0.1 μg/mL proteinase K for 15 minutes at 37°C) were carried out on the Leica BOND-RX. Tissues were incubated with 10% neutral buffered formalin for 5 minutes and 5 minutes with NBF Stop buffer. In situ hybridization with human Whole Transcriptome Assay probes was then carried out overnight in a humidified hybridization chamber kept at 37°C. Following rounds of stringent washing to remove off-target probes, the human breast tissue was blocked with Buffer W blocking solution (NanoString Technologies) then incubated with antibodies for Pan-Cytokeratin (PanCk, Novus, clone: AE1/AE3), CD3E (Origene, clone: UMAB54) and Androgen Receptor (AR, CST, clone: D6F11), as well as with nuclear marker Syto83.

Tissue morphology was visualized using the fluorescent antibodies and Syto83 on the GeoMx® DSP instrument.—Regions of interest (ROIs) were selected from the TMA using either the polygon, rectangle, or circle tool. An AR-high and AR-low ROI were selected from each core. A PanCk+ mask was generated within each ROI using the fluorescence signal associated with the PanCk antibody, and UV light was utilized to release and collect oligonucleotides from each ROI. During PCR, Illumina i5 and i7 dual-indexing primers were added to each Amplified Oligonucleotide Item (AOI) allowing for unique indexing of each AOI. Library concentration was measured using a Qubit fluorometer (Thermo Fisher Scientific), and quality was assessed using a Bioanalyzer (Agilent). The Illumina Novaseq 6000 was used for sequencing, and the resulting FASTQ files were then processed by the NanoString DND pipeline to generate count data for each target probe in every Amplified Oligonucleotide Item (AOI).

Quality control and preprocessing of GeoMx transcript data—The GeoMx DSP Analysis Suite (Version 2.5.1.145) was utilized for conducting both quality control (QC) and data exploration. First, each AOI was QC checked to ensure contamination was avoided during PCR and library preparation and that sequencing was sufficient. No AOIs were eliminated during QC. Next, we checked for global outliers in the target list. No outliers were identified. In total, none of the AOIs nor any of the 18,676 gene-associated probes were removed during QC. Finally, the dataset was normalized using third quantile (Q3) normalization. Differentially expressed genes (AR-hi vs AR-low) are identify by student's t test ($p<0.05$) or paired t test ($p<0.05$). Gene set enrichment analysis is conducted by using the C2 curated gene sets and C8 cell type signature gene sets in the Molecular Signatures Database (MSigDB GSEA 4.3.2). Enriched gene sets are identified by fold discovery rate (FDR q-value<0.05).

AR transactivation—AR transactivation was performed as previously described[29, 31]. Briefly, HEK-293 or COS-7 cells were transfected with plasmid DNA indicated in the figure legends with lipofectamine using OptiMEM medium. Twenty-four hours after transfection,

the cells were fed with DMEM w/o phenol red and treated as indicated in the figures. The cells were harvested 24 hours after treatment and luciferase assay was performed with dual luciferase assay kit (Goldbio, St. Louis, MO).

Co-immunoprecipitation—HEK-293 cells were plated in 10 cm dishes and transfected with lipofectamine as indicated in the figures. Cells were treated with 2000 IU of IFN-α and 10 nM R1881. Cells were harvested 4 hours after treatment and immunoprecipitation was performed as indicated in the figures and previous published[29, 31, 34]. Cells were suspended in lysis buffer (50 mM Tris pH8, 137 mM NaCl, 1% glycerol, 1% NP40, 2 nM EDTA) containing protease and phosphatase inhibitors, and subjected to three freeze-thaw cycles. Protein concentrations were measured by BCA assay. Magnetic beads are washed twice with wash buffer. Protein, lysis buffer, and antibody were then added to the beads. The mixture was rotated and incubated at 4℃ for ~12 hours. After the incubation, the beads were washed three times and then loading dye was added. The crosslinked beads and dye were denatured at 95℃. Equal amounts of protein were fractionated on an SDS-PAGE and transferred to a PVDF membrane. Western blot was performed as previously described[70].

ChIP-PCR—MDA-MB-453 cells were fixed and sheared using a sonicating probe. ChIP assay was performed with STAT1 antibody in MDA-MB-453 cells and, real-time PCR was performed with *CXCL11* promoter (F:GGTTTTCACAGTGCTTTCAC; R:TTTCCCTCTTTGAGTCATGC), *hIL8* promoter (F:GAAAAGTTGTAGTATGCCCC; R:CATGATGGTGAAGATAAGCC), and *FKBP5* regulatory region (F:GCTCCCTCACACCAGATGACCA; R: CAAATCCAACCCGAGACAGGTGTA)[70].

Patient Explant Sponge Culture.—Fresh and frozen in liquid nitrogen in freezing medium patient specimens were used for sponge culture. Sponge cultures were performed in accordance with the protocol published earlier[70, 87–89]. Tumors were cut into small pieces (~1 mm^3) and incubated on pre-soaked gelatin sponges (3 fragments/sponge) in 12 well plates containing 1.5 mL medium (MEM+10% FBS+2 mM L-glutamine + 10 μg/mL insulin + penicillin: streptomycin). The cultures were performed in triplicates. Pooled samples (n=3 fragments/sponge) from each sponge constituted one sample. Medium was replaced the next day and treated as indicated in the figures. After 2 days, BrdU was added to the samples and was incubated for another 8–12 hours. Tissues were harvested and fixed in 4% formalin. Tissue was embedded in FFPE blocks. Immunohistochemistry was for anti-Ki67 was done. Characteristics of the patient specimens used in PDX and in sponge cultures are provided in Table ST1.

Quantification and statistical analysis

All experiments were performed at least three independent times. Statistical analysis was performed using GraphPad Prism. Experiments with two groups were analyzed by Student t-test and experiments with more than two groups were analyzed by One Way ANOVA, followed by Tukey post-hoc analysis. Analysis for RNA sequencing and spatial transcriptomics are provided under the respective sections. Values are expressed as average ±

S.E.* - p<0.05; ** - p<0.01; *** - p<0.001; **** - p<0.0001. Sequencing data are deposited in GEO databank.

Additional resources

None

Supplementary Material

Refer to Web version on PubMed Central for supplementary material.

Acknowledgments:

The authors thank the NCI Division of Cancer Treatment and Diagnosis Stepping Stones program for assistance in acquiring compound and in vitro ADME data for the development of UT-105.

Funding:

This work was supported by research grants from the National Cancer Institute R01-CA229164, R01-CA253329, F30CA265224, Department of Defense (DOD) W81XWH-21-1-0055, Oncternal Therapeutics Inc., San Diego, CA, Eric Muirhead Chair of Excellence, and the UTHSC Center for Cancer Research.

Data and materials availability:

All sequencing data were deposited in a public database. PDXs and cell line models will made available under MTA upon request. Novel proprietary compounds will be shared upon receiving authorization form licensing organizations. All data are available in the main text or the supplementary materials.

References and Notes

1. Siegel RL; Miller KD; Wagle NS; Jemal A, Cancer statistics, 2023. CA: A Cancer Journal for Clinicians 2023, 73 (1), 17–48. [PubMed: 36633525]
2. Perou CM; Sorlie T; Eisen MB; van de Rijn M; Jeffrey SS; Rees CA; Pollack JR; Ross DT; Johnsen H; Akslen LA; Fluge O; Pergamenschikov A; Williams C; Zhu SX; Lonning PE; Borresen-Dale AL; Brown PO; Botstein D, Molecular portraits of human breast tumours. Nature 2000, 406 (6797), 747–52. [PubMed: 10963602]
3. Waks AG; Winer EP, Breast Cancer Treatment. JAMA 2019, 321 (3), 288. [PubMed: 30667505]
4. Lehmann BD; Bauer JA; Chen X; Sanders ME; Chakravarthy AB; Shyr Y; Pietenpol JA, Identification of human triple-negative breast cancer subtypes and preclinical models for selection of targeted therapies. Journal of Clinical Investigation 2011, 121 (7), 2750–2767. [PubMed: 21633166]
5. Morris GJ; Naidu S; Topham AK; Guiles F; Xu Y; McCue P; Schwartz GF; Park PK; Rosenberg AL; Brill K; Mitchell EP, Differences in breast carcinoma characteristics in newly diagnosed African–American and Caucasian patients. Cancer 2007, 110 (4), 876–884. [PubMed: 17620276]
6. Haffty BG; Yang Q; Reiss M; Kearney T; Higgins SA; Weidhaas J; Harris L; Hait W; Toppmeyer D, Locoregional Relapse and Distant Metastasis in Conservatively Managed Triple Negative Early-Stage Breast Cancer. Journal of Clinical Oncology 2006, 24 (36), 5652–5657. [PubMed: 17116942]
7. Mina A; Yoder R; Sharma P, Targeting the androgen receptor in triple-negative breast cancer: current perspectives. OncoTargets and Therapy 2017, *Volume* 10, 4675–4685. [PubMed: 29033586]
8. Choupani E; Mahmoudi Gomari M; Zanganeh S; Nasseri S; Haji-Allahverdipoor K; Rostami N; Hernandez Y; Najafi S; Saraygord-Afshari N; Hosseini A, Newly Developed Targeted Therapies Against the Androgen Receptor in Triple-Negative Breast Cancer: A Review. Pharmacol Rev 2023, 75 (2), 309–327. [PubMed: 36781219]

9. Lehmann BD; Jovanovic B; Chen X; Estrada MV; Johnson KN; Shyr Y; Moses HL; Sanders ME; Pietenpol JA, Refinement of Triple-Negative Breast Cancer Molecular Subtypes: Implications for Neoadjuvant Chemotherapy Selection. PLoS One 2016, 11 (6), e0157368. [PubMed: 27310713]
10. Loibl S; Müller BM; Von Minckwitz G; Schwabe M; Roller M; Darb-Esfahani S; Ataseven B; Du Bois A; Fissler-Eckhoff A; Gerber B; Kulmer U; Alles J-U; Mehta K; Denkert C, Androgen receptor expression in primary breast cancer and its predictive and prognostic value in patients treated with neoadjuvant chemotherapy. Breast Cancer Research and Treatment 2011, 130 (2), 477–487. [PubMed: 21837479]
11. Traina TA; Miller K; Yardley DA; Eakle J; Schwartzberg LS; O'Shaughnessy J; Gradishar W; Schmid P; Winer E; Kelly C; Nanda R; Gucalp A; Awada A; Garcia-Estevez L; Trudeau ME; Steinberg J; Uppal H; Tudor IC; Peterson A; Cortes J, Enzalutamide for the Treatment of Androgen Receptor–Expressing Triple-Negative Breast Cancer. Journal of Clinical Oncology 2018, 36 (9), 884–890. [PubMed: 29373071]
12. Gucalp A; Tolaney S; Isakoff SJ; Ingle JN; Liu MC; Carey LA; Blackwell K; Rugo H; Nabell L; Forero A; Stearns V; Doane AS; Danso M; Moynahan ME; Momen LF; Gonzalez JM; Akhtar A; Giri DD; Patil S; Feigin KN; Hudis CA; Traina TA, Phase II Trial of Bicalutamide in Patients with Androgen Receptor–Positive, Estrogen Receptor–Negative Metastatic Breast Cancer. Clinical Cancer Research 2013, 19 (19), 5505–5512. [PubMed: 23965901]
13. Gucalp A; Traina TA, Androgen receptor-positive, triple-negative breast cancer. Cancer 2017, 123 (10), 1686–1688. [PubMed: 28406524]
14. Schwartzberg LS; Yardley DA; Elias AD; Patel M; LoRusso P; Burris HA; Gucalp A; Peterson AC; Blaney ME; Steinberg JL; Gibbons JA; Traina TA, A Phase I/Ib Study of Enzalutamide Alone and in Combination with Endocrine Therapies in Women with Advanced Breast Cancer. Clin Cancer Res 2017, 23 (15), 4046–4054. [PubMed: 28280092]
15. Zhou ZX; Wong CI; Sar M; Wilson EM, The androgen receptor: an overview. Recent Prog Horm Res 1994, 49, 249–74. [PubMed: 8146426]
16. Lu NZ; Wardell SE; Burnstein KL; Defranco D; Fuller PJ; Giguere V; Hochberg RB; McKay L; Renoir JM; Weigel NL; Wilson EM; McDonnell DP; Cidlowski JA, International Union of Pharmacology. LXV. The pharmacology and classification of the nuclear receptor superfamily: glucocorticoid, mineralocorticoid, progesterone, and androgen receptors. Pharmacol Rev 2006, 58 (4), 782–97. [PubMed: 17132855]
17. Askew EB; Minges JT; Hnat AT; Wilson EM, Structural features discriminate androgen receptor N/C terminal and coactivator interactions. Mol Cell Endocrinol 2012, 348 (2), 403–10. [PubMed: 21664945]
18. Dehm SM; Tindall DJ, Alternatively spliced androgen receptor variants. Endocrine-Related Cancer 2011, 18 (5), R183–R196. [PubMed: 21778211]
19. Wadosky KM; Koochekpour S, Androgen receptor splice variants and prostate cancer: From bench to bedside. Oncotarget 2017, 8 (11), 18550–18576. [PubMed: 28077788]
20. Young FP; Becker TM; Nimir M; Opperman T; Chua W; Balakrishnar B; de Souza P; Ma Y, Biomarkers of Castrate Resistance in Prostate Cancer: Androgen Receptor Amplification and T877A Mutation Detection by Multiplex Droplet Digital PCR. J Clin Med 2022, 11 (1).
21. Antonarakis ES; Lu C; Wang H; Luber B; Nakazawa M; Roeser JC; Chen Y; Mohammad TA; Chen Y; Fedor HL; Lotan TL; Zheng Q; De Marzo AM; Isaacs JT; Isaacs WB; Nadal R; Paller CJ; Denmeade SR; Carducci MA; Eisenberger MA; Luo J, AR-V7 and resistance to enzalutamide and abiraterone in prostate cancer. N Engl J Med 2014, 371 (11), 1028–38. [PubMed: 25184630]
22. Nakazawa M; Antonarakis ES; Luo J, Androgen receptor splice variants in the era of enzalutamide and abiraterone. Horm Cancer 2014, 5 (5), 265–73. [PubMed: 25048254]
23. Kanayama M; Lu C; Luo J; Antonarakis ES, AR Splicing Variants and Resistance to AR Targeting Agents. Cancers (Basel) 2021, 13 (11).
24. Li Y; Chan SC; Brand LJ; Hwang TH; Silverstein KA; Dehm SM, Androgen receptor splice variants mediate enzalutamide resistance in castration-resistant prostate cancer cell lines. Cancer Res 2013, 73 (2), 483–9. [PubMed: 23117885]
25. Mostaghel EA; Marck BT; Plymate SR; Vessella RL; Balk S; Matsumoto AM; Nelson PS; Montgomery RB, Resistance to CYP17A1 inhibition with abiraterone in castration-resistant

prostate cancer: induction of steroidogenesis and androgen receptor splice variants. Clin Cancer Res 2011, 17 (18), 5913–25. [PubMed: 21807635]

26. Zhang G; Liu X; Li J; Ledet E; Alvarez X; Qi Y; Fu X; Sartor O; Dong Y; Zhang H, Androgen receptor splice variants circumvent AR blockade by microtubule-targeting agents. Oncotarget 2015, 6 (27), 23358–71. [PubMed: 26160840]
27. Hickey TE; Irvine CM; Dvinge H; Tarulli GA; Hanson AR; Ryan NK; Pickering MA; Birrell SN; Hu DG; Mackenzie PI; Russell R; Caldas C; Raj GV; Dehm SM; Plymate SR; Bradley RK; Tilley WD; Selth LA, Expression of androgen receptor splice variants in clinical breast cancers. Oncotarget 2015, 6 (42), 44728–44744. [PubMed: 26554309]
28. Lehmann BD; Abramson VG; Sanders ME; Mayer EL; Haddad TC; Nanda R; Van Poznak C; Storniolo AM; Nangia JR; Gonzalez-Ericsson PI; Sanchez V; Johnson KN; Abramson RG; Chen SC; Shyr Y; Arteaga CL; Wolff AC; Pietenpol JA; Translational Breast Cancer Research, C., TBCRC 032 IB/II Multicenter Study: Molecular Insights to AR Antagonist and PI3K Inhibitor Efficacy in Patients with AR(+) Metastatic Triple-Negative Breast Cancer. Clin Cancer Res 2020, 26 (9), 2111–2123. [PubMed: 31822498]
29. Ponnusamy S; Coss CC; Thiyagarajan T; Watts K; Hwang D-J; He Y; Selth LA; McEwan IJ; Duke CB; Pagadala J; Singh G; Wake RW; Ledbetter C; Tilley WD; Moldoveanu T; Dalton JT; Miller DD; Narayanan R, Novel Selective Agents for the Degradation of Androgen Receptor Variants to Treat Castration-Resistant Prostate Cancer. Cancer Research 2017, 77 (22), 6282–6298. [PubMed: 28978635]
30. Tran C; Ouk S; Clegg NJ; Chen Y; Watson PA; Arora V; Wongvipat J; Smith-Jones PM; Yoo D; Kwon A; Wasielewska T; Welsbie D; Chen CD; Higano CS; Beer TM; Hung DT; Scher HI; Jung ME; Sawyers CL, Development of a second-generation antiandrogen for treatment of advanced prostate cancer. Science 2009, 324 (5928), 787–90. [PubMed: 19359544]
31. Ponnusamy S; He Y; Hwang D-J; Thiyagarajan T; Houtman R; Bocharova V; Sumpter BG; Fernandez E; Johnson D; Du Z; Pfeffer LM; Getzenberg RH; McEwan IJ; Miller DD; Narayanan R, Orally Bioavailable Androgen Receptor Degrader, Potential Next-Generation Therapeutic for Enzalutamide-Resistant Prostate Cancer. Clinical Cancer Research 2019, 25 (22), 6764–6780. [PubMed: 31481513]
32. Myung J-K; Banuelos CA; Fernandez JG; Mawji NR; Wang J; Tien AH; Yang YC; Tavakoli I; Haile S; Watt K; McEwan IJ; Plymate S; Andersen RJ; Sadar MD, An androgen receptor N-terminal domain antagonist for treating prostate cancer. Journal of Clinical Investigation 2013, 123 (7), 2948–2960. [PubMed: 23722902]
33. Elgehama A; Sun L; Yu B; Guo W; Xu Q, Selective targeting of the androgen receptor-DNA binding domain by the novel antiandrogen SBF-1 and inhibition of the growth of prostate cancer cells. Investigational New Drugs 2021, 39 (2), 442–457. [PubMed: 33411211]
34. Thiyagarajan T; Ponnusamy S; Hwang DJ; He Y; Asemota S; Young KL; Johnson DL; Bocharova V; Zhou W; Jain AK; Petricoin EF; Yin Z; Pfeffer LM; Miller DD; Narayanan R, Inhibiting androgen receptor splice variants with cysteine-selective irreversible covalent inhibitors to treat prostate cancer. Proc Natl Acad Sci U S A 2023, 120 (1), e2211832120. [PubMed: 36577061]
35. He Y; Hwang D-J; Ponnusamy S; Thiyagarajan T; Mohler ML; Narayanan R; Miller DD, Pyrazol-1-yl-propanamides as SARD and Pan-Antagonists for the Treatment of Enzalutamide-Resistant Prostate Cancer. Journal of Medicinal Chemistry 2020, 63 (21), 12642–12665. [PubMed: 33095584]
36. He Y; Hwang DJ; Ponnusamy S; Thiyagarajan T; Mohler ML; Narayanan R; Miller DD, Exploration and Biological Evaluation of Basic Heteromonocyclic Propanamide Derivatives as SARDs for the Treatment of Enzalutamide-Resistant Prostate Cancer. J Med Chem 2021, 64 (15), 11045–11062. [PubMed: 34269581]
37. Hwang D-J; He Y; Ponnusamy S; Mohler ML; Thiyagarajan T; McEwan IJ; Narayanan R; Miller DD, New Generation of Selective Androgen Receptor Degraders: Our Initial Design, Synthesis, and Biological Evaluation of New Compounds with Enzalutamide-Resistant Prostate Cancer Activity. Journal of Medicinal Chemistry 2019, 62 (2), 491–511. [PubMed: 30525603]
38. Hwang DJ; He Y; Ponnusamy S; Thiyagarajan T; Mohler ML; Narayanan R; Miller DD, Metabolism-Guided Selective Androgen Receptor Antagonists: Design, Synthesis, and Biological

Evaluation for Activity against Enzalutamide-Resistant Prostate Cancer. J Med Chem 2023, 66 (5), 3372–3392. [PubMed: 36825758]

39. Andersen RJ; Mawji NR; Wang J; Wang G; Haile S; Myung J-K; Watt K; Tam T; Yang YC; Bañuelos CA; Williams DE; McEwan IJ; Wang Y; Sadar MD, Regression of Castrate-Recurrent Prostate Cancer by a Small-Molecule Inhibitor of the Amino-Terminus Domain of the Androgen Receptor. Cancer Cell 2010, 17 (6), 535–546. [PubMed: 20541699]
40. Deng S; Wang C; Wang Y; Xu Y; Li X; Johnson NA; Mukherji A; Lo UG; Xu L; Gonzalez J; Metang LA; Ye J; Tirado CR; Rodarte K; Zhou Y; Xie Z; Arana C; Annamalai V; Liu X; Vander Griend DJ; Strand D; Hsieh J-T; Li B; Raj G; Wang T; Mu P, Ectopic JAK–STAT activation enables the transition to a stem-like and multilineage state conferring AR-targeted therapy resistance. Nature Cancer 2022.
41. Chan JM; Zaidi S; Love JR; Zhao JL; Setty M; Wadosky KM; Gopalan A; Choo ZN; Persad S; Choi J; LaClair J; Lawrence KE; Chaudhary O; Xu T; Masilionis I; Linkov I; Wang S; Lee C; Barlas A; Morris MJ; Mazutis L; Chaligne R; Chen Y; Goodrich DW; Karthaus WR; Pe'er D; Sawyers CL, Lineage plasticity in prostate cancer depends on JAK/STAT inflammatory signaling. Science 2022, 377 (6611), 1180–1191. [PubMed: 35981096]
42. Fleming SB, Viral Inhibition of the IFN-Induced JAK/STAT Signalling Pathway: Development of Live Attenuated Vaccines by Mutation of Viral-Encoded IFN-Antagonists. Vaccines (Basel) 2016, 4 (3).
43. Gotthardt D; Trifinopoulos J; Sexl V; Putz EM, JAK/STAT Cytokine Signaling at the Crossroad of NK Cell Development and Maturation. Front Immunol 2019, 10, 2590. [PubMed: 31781102]
44. Beinhoff P; Sabharwal L; Udhane V; Maranto C; LaViolette PS; Jacobsohn KM; Tsai S; Iczkowski KA; Wang L; Hall WA; Dehm SM; Kilari D; Nevalainen MT, Second-Generation Jak2 Inhibitors for Advanced Prostate Cancer: Are We Ready for Clinical Development? Cancers (Basel) 2021, 13 (20).
45. Cochrane DR; Bernales S; Jacobsen BM; Cittelly DM; Howe EN; D'Amato NC; Spoelstra NS; Edgerton SM; Jean A; Guerrero J; Gómez F; Medicherla S; Alfaro IE; McCullagh E; Jedlicka P; Torkko KC; Thor AD; Elias AD; Protter AA; Richer JK, Role of the androgen receptor in breast cancer and preclinical analysis of enzalutamide. Breast Cancer Research 2014, 16 (1), R7. [PubMed: 24451109]
46. Lánczky A; Győrffy B, Web-Based Survival Analysis Tool Tailored for Medical Research (KMplot): Development and Implementation. Journal of Medical Internet Research 2021, 23 (7), e27633. [PubMed: 34309564]
47. Sturtz LA; Melley J; Mamula K; Shriver CD; Ellsworth RE, Outcome disparities in African American women with triple negative breast cancer: a comparison of epidemiological and molecular factors between African American and Caucasian women with triple negative breast cancer. BMC Cancer 2014, 14 (1), 62. [PubMed: 24495414]
48. Rana PS; Wang W; Alkrekshi A; Markovic V; Khiyami A; Chan R; Perzynski A; Joseph N; Sossey-Alaoui K, YB1 Is a Major Contributor to Health Disparities in Triple Negative Breast Cancer. Cancers (Basel) 2021, 13 (24).
49. Lehmann BD; Bauer JA; Chen X; Sanders ME; Chakravarthy AB; Shyr Y; Pietenpol JA, Identification of human triple-negative breast cancer subtypes and preclinical models for selection of targeted therapies. J Clin Invest 2011, 121 (7), 2750–67. [PubMed: 21633166]
50. Luo X; Shi YX; Li ZM; Jiang WQ, Expression and clinical significance of androgen receptor in triple negative breast cancer. Chin J Cancer 2010, 29 (6), 585–90. [PubMed: 20507730]
51. Zhang X; Morrissey C; Sun S; Ketchandji M; Nelson PS; True LD; Vakar-Lopez F; Vessella RL; Plymate SR, Androgen Receptor Variants Occur Frequently in Castration Resistant Prostate Cancer Metastases. PLoS ONE 2011, 6 (11), e27970. [PubMed: 22114732]
52. Khan F; Anelo OM; Sadiq Q; Effah W; Price G; Johnson DL; Ponnusamy S; Grimes B; Morrison ML; Fowke JH; Hayes DN; Narayanan R, Racial Differences in Androgen Receptor (AR) and AR Splice Variants (AR-SVs) Expression in Treatment-Naïve Androgen-Dependent Prostate Cancer. Biomedicines 2023, 11 (3), 648. [PubMed: 36979627]
53. Martz CA; Ottina KA; Singleton KR; Jasper JS; Wardell SE; Peraza-Penton A; Anderson GR; Winter PS; Wang T; Alley HM; Kwong LN; Cooper ZA; Tetzlaff M; Chen PL; Rathmell JC; Flaherty KT; Wargo JA; McDonnell DP; Sabatini DM; Wood KC, Systematic identification of

signaling pathways with potential to confer anticancer drug resistance. Sci Signal 2014, 7 (357), ra121. [PubMed: 25538079]

54. Doane AS; Danso M; Lal P; Donaton M; Zhang L; Hudis C; Gerald WL, An estrogen receptor-negative breast cancer subset characterized by a hormonally regulated transcriptional program and response to androgen. Oncogene 2006, 25 (28), 3994–4008. [PubMed: 16491124]
55. Bell LA; Ryan KM, Life and death decisions by E2F-1. Cell Death & Differentiation 2004, 11 (2), 137–142. [PubMed: 14526389]
56. Johnson J; Thijssen B; McDermott U; Garnett M; Wessels LFA; Bernards R, Targeting the RB-E2F pathway in breast cancer. Oncogene 2016, 35 (37), 4829–4835. [PubMed: 26923330]
57. Balbas MD; Evans MJ; Hosfield DJ; Wongvipat J; Arora VK; Watson PA; Chen Y; Greene GL; Shen Y; Sawyers CL, Overcoming mutation-based resistance to antiandrogens with rational drug design. Elife 2013, 2, e00499. [PubMed: 23580326]
58. Huynh K; Partch CL, Analysis of Protein Stability and Ligand Interactions by Thermal Shift Assay. Current Protocols in Protein Science 2015, 79 (1).
59. Kopra K; Valtonen S; Mahran R; Kapp JN; Hassan N; Gillette W; Dennis B; Li L; Westover KD; Pluckthun A; Harma H, Thermal Shift Assay for Small GTPase Stability Screening: Evaluation and Suitability. Int J Mol Sci 2022, 23 (13).
60. Wright PE; Dyson HJ, Intrinsically unstructured proteins: re-assessing the protein structure-function paradigm. J Mol Biol 1999, 293 (2), 321–31. [PubMed: 10550212]
61. Martinez Molina D; Jafari R; Ignatushchenko M; Seki T; Larsson EA; Dan C; Sreekumar L; Cao Y; Nordlund P, Monitoring drug target engagement in cells and tissues using the cellular thermal shift assay. Science 2013, 341 (6141), 84–7. [PubMed: 23828940]
62. Vedadi M; Niesen FH; Allali-Hassani A; Fedorov OY; Finerty PJ Jr.; Wasney GA; Yeung R; Arrowsmith C; Ball LJ; Berglund H; Hui R; Marsden BD; Nordlund P; Sundstrom M; Weigelt J; Edwards AM, Chemical screening methods to identify ligands that promote protein stability, protein crystallization, and structure determination. Proc Natl Acad Sci U S A 2006, 103 (43), 15835–40. [PubMed: 17035505]
63. Barrault C; Garnier J; Pedretti N; Cordier-Dirikoc S; Ratineau E; Deguercy A; Bernard FX, Androgens induce sebaceous differentiation in sebocyte cells expressing a stable functional androgen receptor. J Steroid Biochem Mol Biol 2015, 152, 34–44. [PubMed: 25864624]
64. Averboukh L; Liang P; Kantoff PW; Pardee AB, Regulation of S100P expression by androgen. Prostate 1996, 29 (6), 350–5. [PubMed: 8977631]
65. Kojima S; Mulholland DJ; Ettinger S; Fazli L; Nelson CC; Gleave ME, Differential regulation of IGFBP-3 by the androgen receptor in the lineage-related androgen-dependent LNCaP and androgen-independent C4–2 prostate cancer models. Prostate 2006, 66 (9), 971–86. [PubMed: 16541420]
66. Pang ST; Dillner K; Wu X; Pousette A; Norstedt G; Flores-Morales A, Gene expression profiling of androgen deficiency predicts a pathway of prostate apoptosis that involves genes related to oxidative stress. Endocrinology 2002, 143 (12), 4897–906. [PubMed: 12446617]
67. Asirvatham AJ; Schmidt M; Gao B; Chaudhary J, Androgens regulate the immune/inflammatory response and cell survival pathways in rat ventral prostate epithelial cells. Endocrinology 2006, 147 (1), 257–71. [PubMed: 16195407]
68. Zhang L; Zhao Z; Xu S; Tandon M; LaValle CR; Deng F; Wang QJ, Androgen suppresses protein kinase D1 expression through fibroblast growth factor receptor substrate 2 in prostate cancer cells. Oncotarget 2017, 8 (8), 12800–12811. [PubMed: 28077787]
69. Wach S; Taubert H; Cronauer M, Role of androgen receptor splice variants, their clinical relevance and treatment options. World Journal of Urology 2020, 38 (3), 647–656. [PubMed: 30659302]
70. Ponnusamy S; Asemota S; Schwartzberg LS; Guestini F; McNamara KM; Pierobon M; Font-Tello A; Qiu X; Xie Y; Rao PK; Thiyagarajan T; Grimes B; Johnson DL; Fleming MD; Pritchard FE; Berry MP; Oswaks R; Fine RE; Brown M; Sasano H; Petricoin EF; Long HW; Narayanan R, Androgen Receptor Is a Non-canonical Inhibitor of Wild-Type and Mutant Estrogen Receptors in Hormone Receptor-Positive Breast Cancers. iScience 2019, 21, 341–358. [PubMed: 31698248]
71. Cochrane DR; Bernales S; Jacobsen BM; Cittelly DM; Howe EN; NC DA; Spoelstra NS; Edgerton SM; Jean A; Guerrero J; Gomez F; Medicherla S; Alfaro IE; McCullagh E; Jedlicka P; Torkko

KC; Thor AD; Elias AD; Protter AA; Richer JK, Role of the Androgen Receptor in Breast Cancer and Preclinical Analysis of Enzalutamide. Breast Cancer Res 2014, 16 (1), R7. [PubMed: 24451109]

72. Wilson S; Qi J; Filipp FV, Refinement of the androgen response element based on ChIP-Seq in androgen-insensitive and androgen-responsive prostate cancer cell lines. Sci Rep 2016, 6, 32611. [PubMed: 27623747]
73. Platanias LC, Mechanisms of type-I- and type-II-interferon-mediated signalling. Nature Reviews Immunology 2005, 5 (5), 375–386.
74. Pestka S; Langer JA; Zoon KC; Samuel CE, Interferons and their actions. Annu Rev Biochem 1987, 56, 727–77. [PubMed: 2441659]
75. Jorgovanovic D; Song M; Wang L; Zhang Y, Roles of IFN-gamma in tumor progression and regression: a review. Biomark Res 2020, 8, 49. [PubMed: 33005420]
76. Quintas-Cardama A; Vaddi K; Liu P; Manshouri T; Li J; Scherle PA; Caulder E; Wen X; Li Y; Waeltz P; Rupar M; Burn T; Lo Y; Kelley J; Covington M; Shepard S; Rodgers JD; Haley P; Kantarjian H; Fridman JS; Verstovsek S, Preclinical characterization of the selective JAK1/2 inhibitor INCB018424: therapeutic implications for the treatment of myeloproliferative neoplasms. Blood 2010, 115 (15), 3109–17. [PubMed: 20130243]
77. Mesa RA; Yasothan U; Kirkpatrick P, Ruxolitinib. Nat Rev Drug Discov 2012, 11 (2), 103–4. [PubMed: 22293561]
78. Lu S-H; Tsai W-S; Chang Y-H; Chou T-Y; Pang S-T; Lin P-H; Tsai C-M; Chang Y-C, Identifying cancer origin using circulating tumor cells. Cancer Biology & Therapy 2016, 17 (4), 430–438. [PubMed: 26828696]
79. Yang Y; Li J; Mao S; Zhu H, Comparison of immunohistology using pan-CK and EMA in the diagnosis of lymph node metastasis of gastric cancer, particularly micrometastasis and isolated tumor cells. Oncology Letters 2013, 5 (3), 768–772. [PubMed: 23426024]
80. Garcia-Diaz A; Shin DS; Moreno BH; Saco J; Escuin-Ordinas H; Rodriguez GA; Zaretsky JM; Sun L; Hugo W; Wang X; Parisi G; Saus CP; Torrejon DY; Graeber TG; Comin-Anduix B; Hu-Lieskovan S; Damoiseaux R; Lo RS; Ribas A, Interferon Receptor Signaling Pathways Regulating PD-L1 and PD-L2 Expression. Cell Reports 2017, 19 (6), 1189–1201. [PubMed: 28494868]
81. Yang M-Q; Du Q; Varley PR; Goswami J; Liang Z; Wang R; Li H; Stolz DB; Geller DA, Interferon regulatory factor 1 priming of tumour-derived exosomes enhances the antitumour immune response. British Journal of Cancer 2018, 118 (1), 62–71. [PubMed: 29112686]
82. Massihnia D; Galvano A; Fanale D; Perez A; Castiglia M; Incorvaia L; Listì A; Rizzo S; Cicero G; Bazan V; Castorina S; Russo A, Triple negative breast cancer: shedding light onto the role of pi3k/akt/mtor pathway. Oncotarget 2016, 7 (37), 60712–60722. [PubMed: 27474173]
83. Costa RLB; Han HS; Gradishar WJ, Targeting the PI3K/AKT/mTOR pathway in triple-negative breast cancer: a review. Breast Cancer Research and Treatment 2018, 169 (3), 397–406. [PubMed: 29417298]
84. Yang C; Wang Y; Sims MM; He Y; Miller DD; Pfeffer LM, Targeting the Bromodomain of BRG-1/BRM Subunit of the SWI/SNF Complex Increases the Anticancer Activity of Temozolomide in Glioblastoma. Pharmaceuticals (Basel) 2021, 14 (9).
85. Wang Y; Yang C; Sims MM; Sacher JR; Raje M; Deokar H; Yue P; Turkson J; Buolamwini JK; Pfeffer LM, SS-4 is a highly selective small molecule inhibitor of STAT3 tyrosine phosphorylation that potently inhibits GBM tumorigenesis in vitro and in vivo. Cancer Lett 2022, 533, 215614. [PubMed: 35245627]
86. Ganguly D; Fan M; Yang CH; Zbytek B; Finkelstein D; Roussel MF; Pfeffer LM, The critical role that STAT3 plays in glioma-initiating cells: STAT3 addiction in glioma. Oncotarget 2018, 9 (31), 22095–22112. [PubMed: 29774125]
87. Ochnik AM; Moore NL; Jankovic-Karasoulos T; Bianco-Miotto T; Ryan NK; Thomas MR; Birrell SN; Butler LM; Tilley WD; Hickey TE, Antiandrogenic actions of medroxyprogesterone acetate on epithelial cells within normal human breast tissues cultured ex vivo. Menopause 2014, 21 (1), 79–88. [PubMed: 23715406]

88. Dean JL; McClendon AK; Hickey TE; Butler LM; Tilley WD; Witkiewicz AK; Knudsen ES, Therapeutic response to CDK4/6 inhibition in breast cancer defined by ex vivo analyses of human tumors. Cell Cycle 2012, 11 (14), 2756–61. [PubMed: 22767154]

89. Hu DG; Selth LA; Tarulli GA; Meech R; Wijayakumara D; Chanawong A; Russell R; Caldas C; Robinson JL; Carroll JS; Tilley WD; Mackenzie PI; Hickey TE, Androgen and Estrogen Receptors in Breast Cancer Coregulate Human UDP-Glucuronosyltransferases 2B15 and 2B17. Cancer Res 2016, 76 (19), 5881–5893. [PubMed: 27496708]

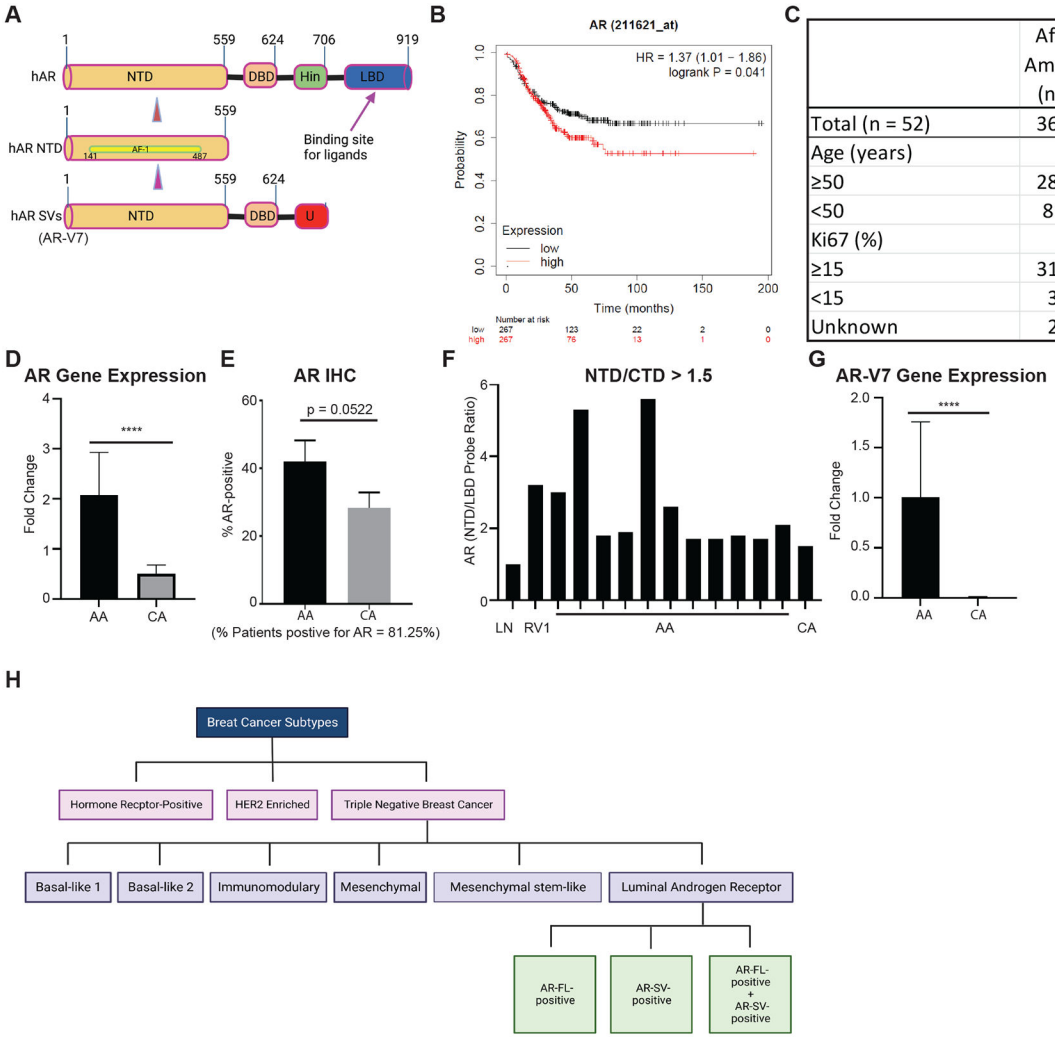

Figure 1: TNBC specimens express full length AR at higher rate and AR splice variants (AR-SV).

A. Structure of AR and AR-SV (biorender.com). **B.** Kaplan Meier relapse free survival plot of patients with high (red) and low (black) AR (211621_at) expression (kmplot.com). **C.** Patient demographics. **D-G.** AR and AR-SV gene expression in specimens from TNBC patients. RNA was extracted (n=52) from TNBC patient specimens and real-time PCR was performed with AR-NTD -binding probe (**D**), AR-NTD - and LBD-binding taqman probes (**F**), and AR-V7 probe (**G**). IHC was performed with AR NTD -binding antibody (**E**). Percent of patients positive for AR (>10% cells positive for AR) is shown at the bottom of the graph. **H.** Flow chart of breast cancer subtypes and TNBC subtypes, including AR-SV-positive TNBC. IHC- immunohistochemistry; NTD- N-terminus domain; CTD- C-terminus domain; AA- African American; CA-Caucasian American; DBD- DNA binding domain; Hin- Hinge; LBD- Ligand Binding Domain; U- Unique cryptic exon; AF-1- Activation Function-1 Domain; AR-FL- androgen receptor full length; AR-SV- androgen receptor splice variant; RV1– 22RV1 prostate cancer cells; LN- LNCaP prostate cancer cells. Values are expressed as mean -/+ SEM. *-p<0.05; **-p<0.01; ***-p<0.001; ****-p<0.0001 (t-test).

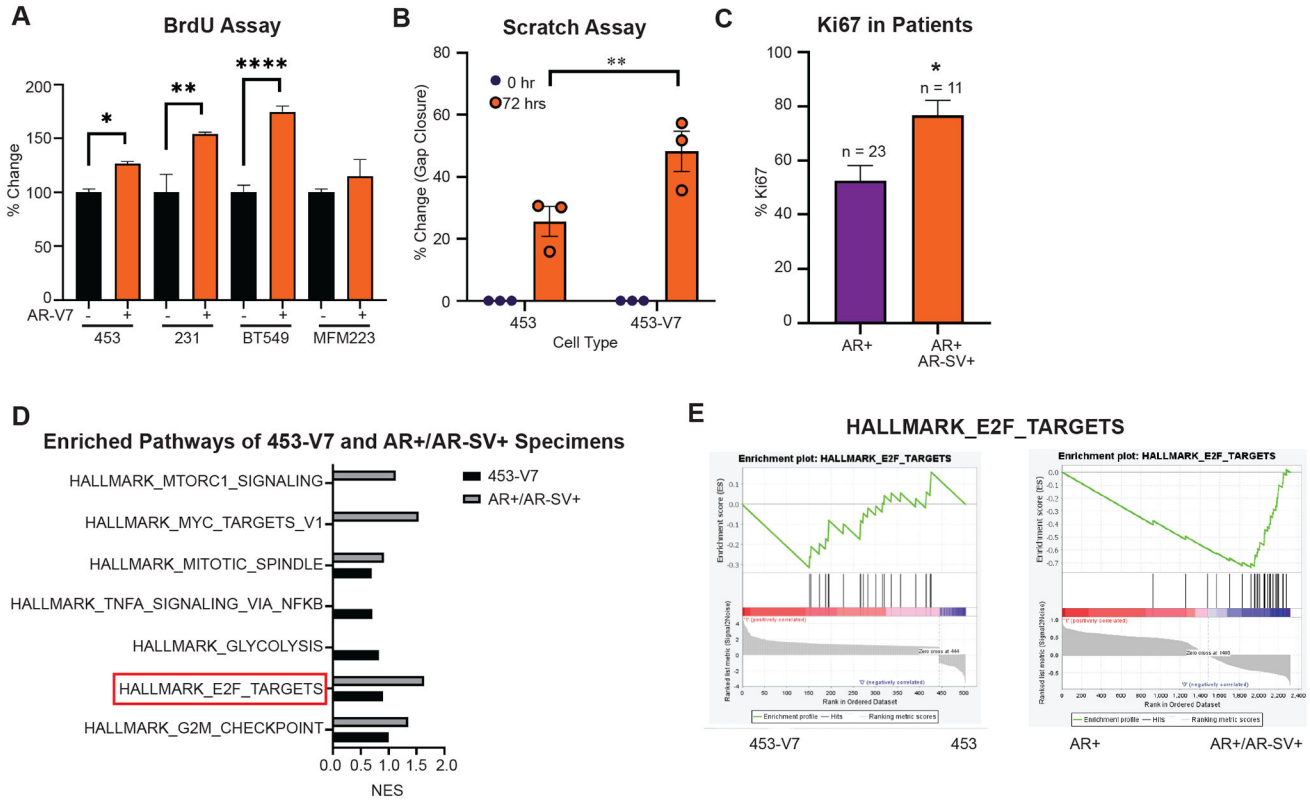

Figure 2: AR-V7 enriches E2F signaling and increases proliferation, invasion, and migration of TNBC cell lines.

TNBC cell lines were stably transfected with AR-V7 using lentivirus. **A.** BrdU assay of control and AR-V7 lentivirus transfected TNBC cell lines MDA-MB-453 (453), MDA-MB-231 (231), BT549, and MFM223. Cells were plated in growth medium and BrDU assay was performed after 72 hours (n=4/group). **B.** Scratch assay in MDA-MB-453 and MDA-MB-453-V7. Cells were plated in growth medium and imaged at the start and after 72 hours, and the gap closure measured by imaging software (n=4/group). **C.** Ki67 staining of TNBC patient specimens (23 (AR-positive (AR+)), and 11 (AR and AR-SV -positive (AR+/AR-SV+)). **D and E.** RNA sequencing was performed with 453 and 453-V7 cell lines and AR+ and AR+/AR-SV+ patient specimens. Gene set from the Molecular Signatures Database is reported in 453 cells compared to 453-V7 cells and AR+ patient specimens compared to AR+/AR-SV+ patient specimens. Values are expressed as mean -/+ SEM. Experiments in panels A-C were reproduced at least three times and representative experiment is shown. * $p<0.05$, ** $p<0.01$, **** $p<0.00001$ (t-test).

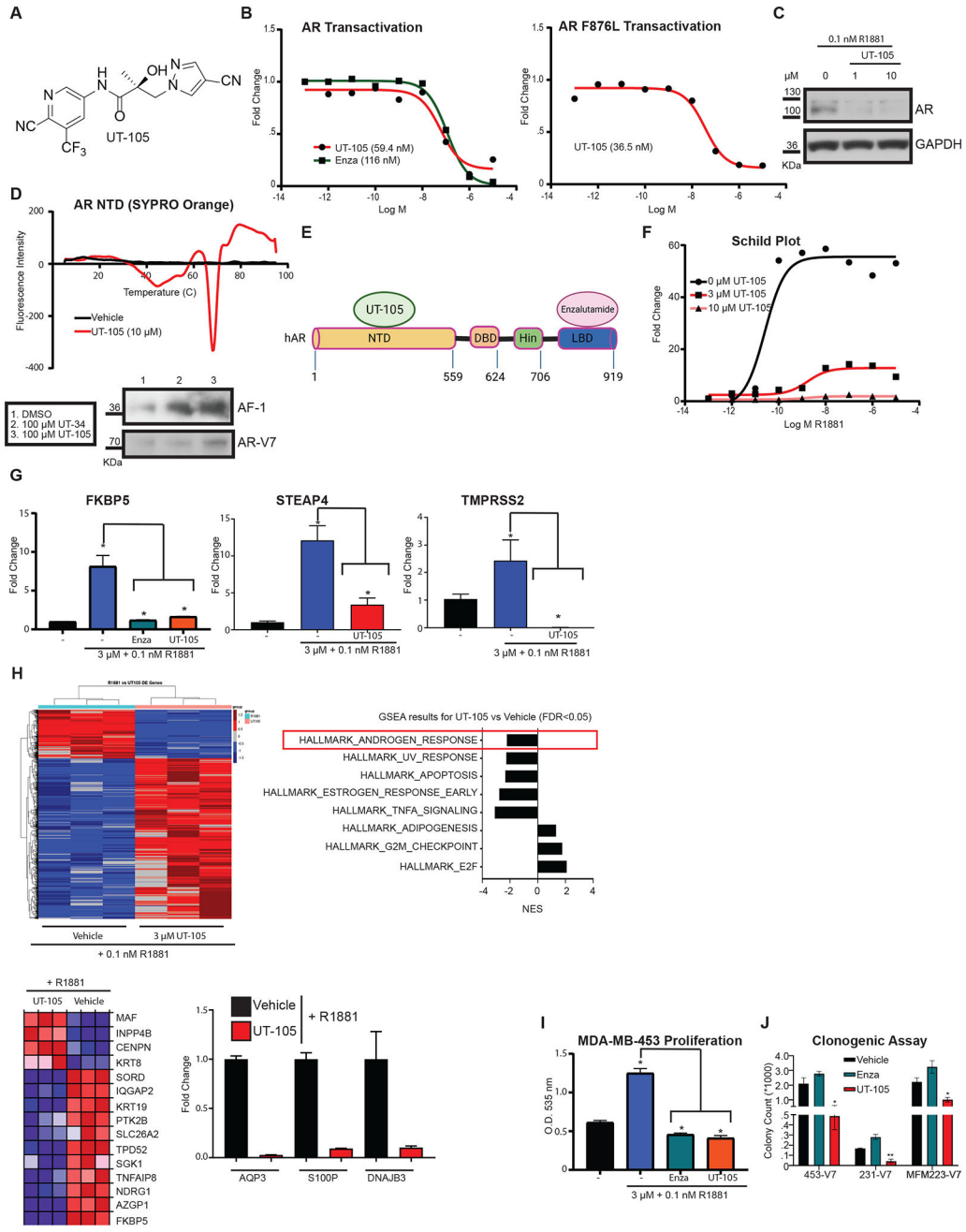

Figure 3: N-terminus-binding AR degrader UT-105 efficiently degrades and irreversibly inhibits AR function in TNBC cell lines.

A. Structure of UT-105**. B**. UT-105 inhibits wildtype and mutant AR transactivation. AR or AR F876L (50 ng), 0.25 μg GRE-LUC, and 10 ng CMV-renilla-LUC were transfected into COS7 cells. Cells were treated 24 hours after transfection with a dose response of UT-105 or enzalutamide in the presence of 0.1 nM R1881, and luciferase assay was performed 24 hours after treatment. Firefly luciferase values were normalized to renilla luciferase. Numbers provided in bracket are IC_{50} values. **C**. UT-105 degrades AR. LNCaP PCa cells were maintained in charcoal-stripped FBS-containing medium for 2 days before treating with UT-105 in the presence of 0.1 nM R1881. Cells were harvested 24 hours after treatment,

and Western blot for AR and GAPDH was performed. **D**. **Top**. UT-105 binds to AR-NTD. Recombinant purified AR NTD was incubated with DMSO or 10 μM UT-105 overnight at 4°C. SYPRO orange dye was added to the mixture and a PCR was performed with increasing temperature. SYPRO orange signal was monitored. **Bottom**. UT-105 stabilized purified AF-1 and AR-V7 recombinant protein. Recombinant purified AF-1 or AR-V7 protein (5 ng) were incubated at room temperature for 4 hours with DMSO or 100 μM of UT-105 or UT-34. Proteins were fractionated on an SDS-PAGE and Western blot was performed with AR antibody (AR-441). **E**. Illustration depicting the binding regions of UT-105 and enzalutamide. **F**. UT-105 irreversibly inhibits AR. Transactivation assay was performed with AR with a dose response of R1881 in the presence of 3 and 10 μM UT-105 as indicated in panel **B**. **G**. UT-105 inhibits AR-target genes. MDA-MB-453 cells in charcoal stripped serum-containing medium were treated for 16–20 hours. RNA was extracted and expression of *FKBP5*, *TMPRSS2*, and *STEAP4* was quantified by real-time PCR and normalized to *GAPDH* (n=4/group). * $p<0.05$ (one-way ANOVA) **H**. RNA-seq. MDA-MB-453 cells maintained in charcoal-stripped serum-containing medium for 2 days were treated with vehicle or 3 μM UT-105 in the presence of 0.1 nM R1881 for 20 hours (n=3/group). Cells were harvested, RNA extracted, and sequenced. Heatmap of global gene expression changes, top GSEA pathways enriched, and heatmap and bar graphs of AR signaling pathway are represented. **I.** UT-105 inhibits proliferation of TNBC cells. MDA-MB-453 cells plated in charcoal stripped serum-containing medium and treated for seven days with medium change and retreatment after day 3 (n=3/group). Sulforhodamine B (SRB) colorimetric assay was performed to measure cell viability. **J.** UT-105 inhibits clonogenicity. TNBC cells stably expressing AR-V7 were plated in 6-well plates and treated with 10 μM of the indicated compounds for two weeks. Colonies were imaged and the number of colonies formed was counted using an imaging software (n=4/group). Panels B-D and F, G, I-J are representatives of at least three independent replicates. * $p<0.05$, ** $p<0.01$ (one-way ANOVA). Enza- enzalutamide; V7- AR-V7 splice variant. Values are expressed as mean -/+ SEM.

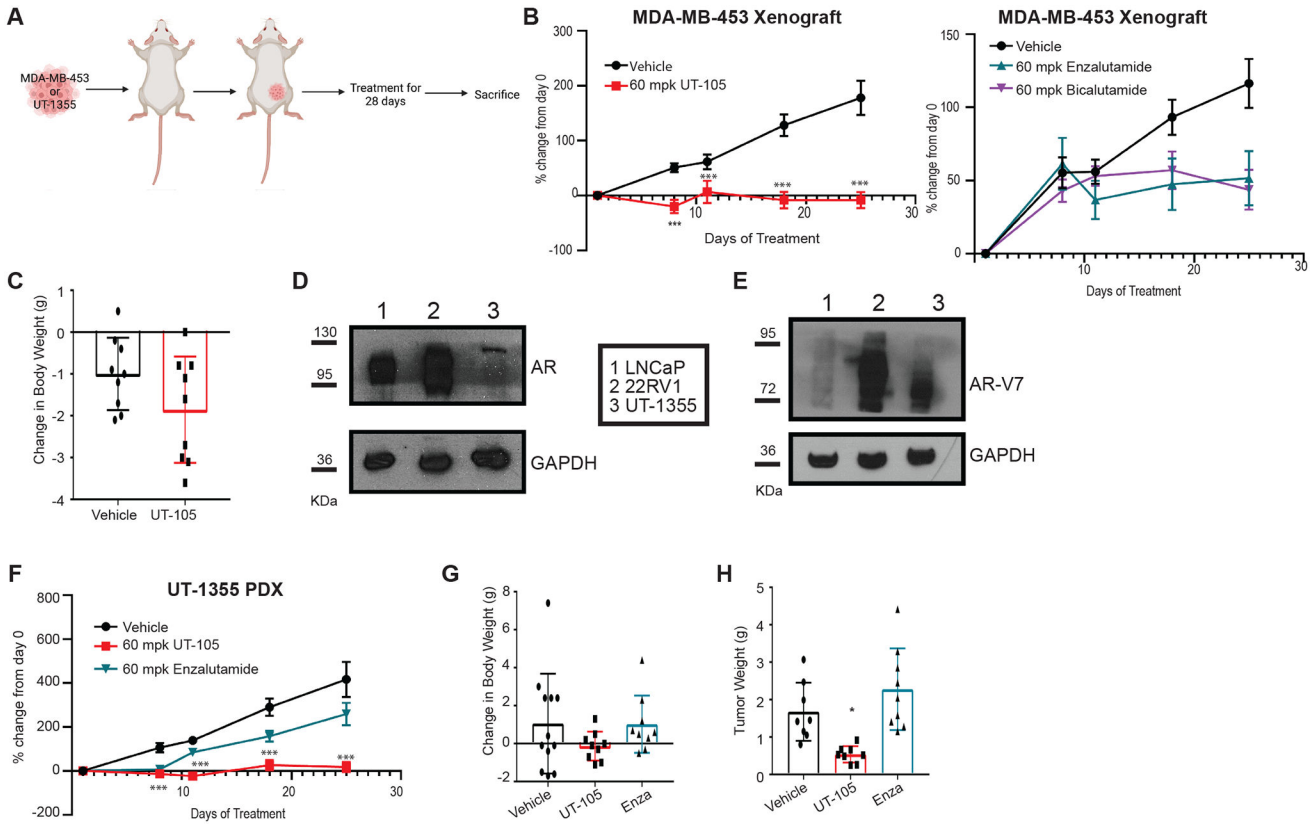

Figure 4: UT-105, but not LBD-binding AR antagonists, inhibits TNBC tumor growth.

A. Schematic representation of CDX and PDX experiments (biorender.com). **B. Left.** MDA-MB-453 orthotopic xenograft was conducted by implanting 5 million cells into the mammary fat pad of female NSG mice. Once the tumors reach 100–300 mm^3, the animals (n=8–10/group) were randomized and treated orally with UT-105 (60 mg/kg/day) or vehicle control (DMSO + PEG-300) for 28 days. Tumor volume was measured by digital caliper twice weekly and the percent change in tumor volume is represented in the graph. **Right.** MDA-MB-453 tumor-bearing female NSG mice (n=8–10/group) were treated with enzalutamide (60 mg/kg/day), bicalutamide (60 mg/kg/day), or vehicle control for 28 days. **C.** Change in body weight of MDA-MB-453 tumor-bearing mice. **D-E.** UT-1355 TNBC PDX characterization. Protein was extracted from UT-1355 PDX tumor fragments and Western blot with AR NTD-binding antibody or AR-V7 antibody, and GAPDH antibody was performed. LNCaP and 22RV1 prostate cancer cells were used as control for AR and AR-SV, respectively. Representative blots shown. **F.** UT-105 completely inhibits UT-1355 PDX tumor growth. UT-1355 PDX tumor fragments (1 mm^3) were orthotopically implanted into the mammary fat pad in female NSG mice (n=8–10/group), and a xenograft experiment was performed as indicated above for MDA-MB-453. **G-H.** Change in body weight of UT-1355-bearing mice and tumor weight. Mean -/+ SEM is shown with One way ANOVA conducted in Graph Pad Prism: * $p<0.05$, ** $p<0.01$, *** $p<0.001$.

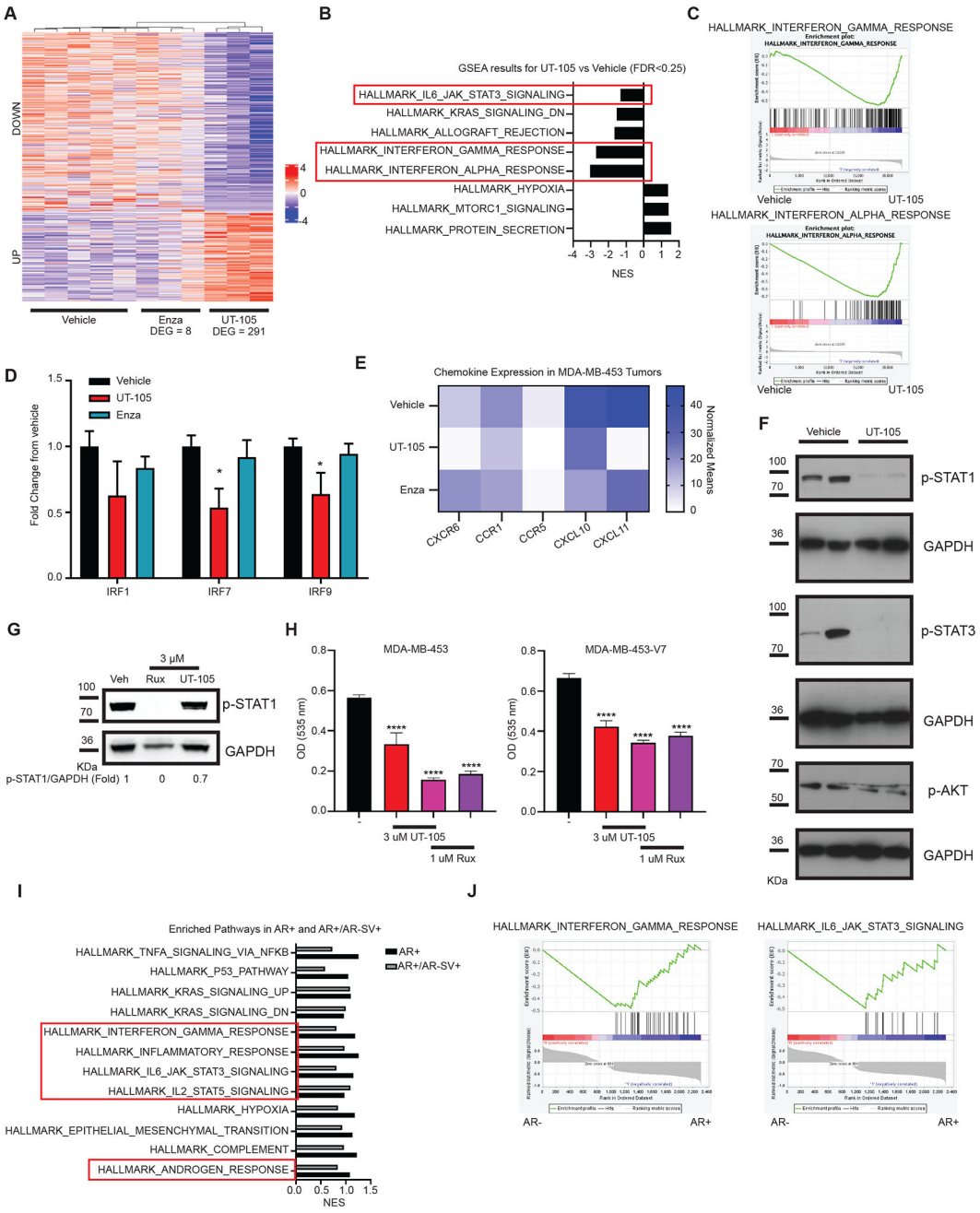

Figure 5: JAK-STAT signaling enriched in LAR-TNBC was inhibited by UT-105.

(A-F) RNA was extracted from MDA-MB-453 tumors (shown in Fig. 4B) and sequenced (n = 3–5/group). **A.** Differentially expressed genes (DEGs) are visualized as a heatmap. The number of significant DEGs in each treatment compared to the vehicle control is shown below. **B.** GSEA analysis was performed on UT-105-treated tumors. Pathways with an FDR<0.25 are shown with corresponding normalized enrichment scores (NES). **C.** Enrichment plots are shown for interferon ɣ (top) and interferon α (bottom) Hallmark response pathways. **D.** Fold change in gene expression from RNA sequencing with MDA-MB-453 tumors for STAT signaling pathway genes *IRF1*, *IRF7*, and *IRF9* is shown.

E. A heatmap of chemokine normalized means from the RNA-seq data performed in MDA-MB-453 xenograft tumors. **F.** Western immunoblot of phospho-STAT1, phospho-STAT3, and phospho-AKT in representative samples from vehicle and UT-105-treated MDA-MB-453 xenograft tumors (from Fig 4B). **G**. Effect of UT-105 and ruxolitinib on STAT1 phosphorylation in MDA-MB-453 cells. MDA-MB-453 cells were maintained in csFBS-containing medium for 48 hours. Cells were treated with 3 μM UT-105 or ruxolitinib for 24 hours before the induction of STAT1 phosphorylation with interferon α (1000 units). Cells were harvested 30 minutes after induction, protein was extracted, and Western blot for pSTAT1 and GAPDH was performed. Representative blot is shown. The bands were quantified and fold change from vehicle is provided under the blots. **H.** Effect of UT-105 and ruxolitinib on cell proliferation. Cells were plated in growth medium and treated with vehicle, UT-105, or JAK-STAT inhibitor ruxolitinib for seven days with medium change and retreatment after day 3 (n=4/group; representative of three replicates; one-way ANOVA). SRB assay was performed. **I**. AR and AR-SV -positive TNBC specimens are enriched for JAK-STAT pathway. RNA was extracted from TNBC specimens (n=41) shown in Fig. 1C and sequenced. The top pathways enriched in AR and AR-SV compared to AR negative specimens obtained from GSEA (FDR <0.25) are shown as a bar graph. **J.** Enrichment plots are shown. Rux- ruxolitinib; enza- enzalutamide. Mean -/+ SEM: * $p<0.05$, ** $p<0.01$, *** $p<0.001$, **** $p<0.00001$.

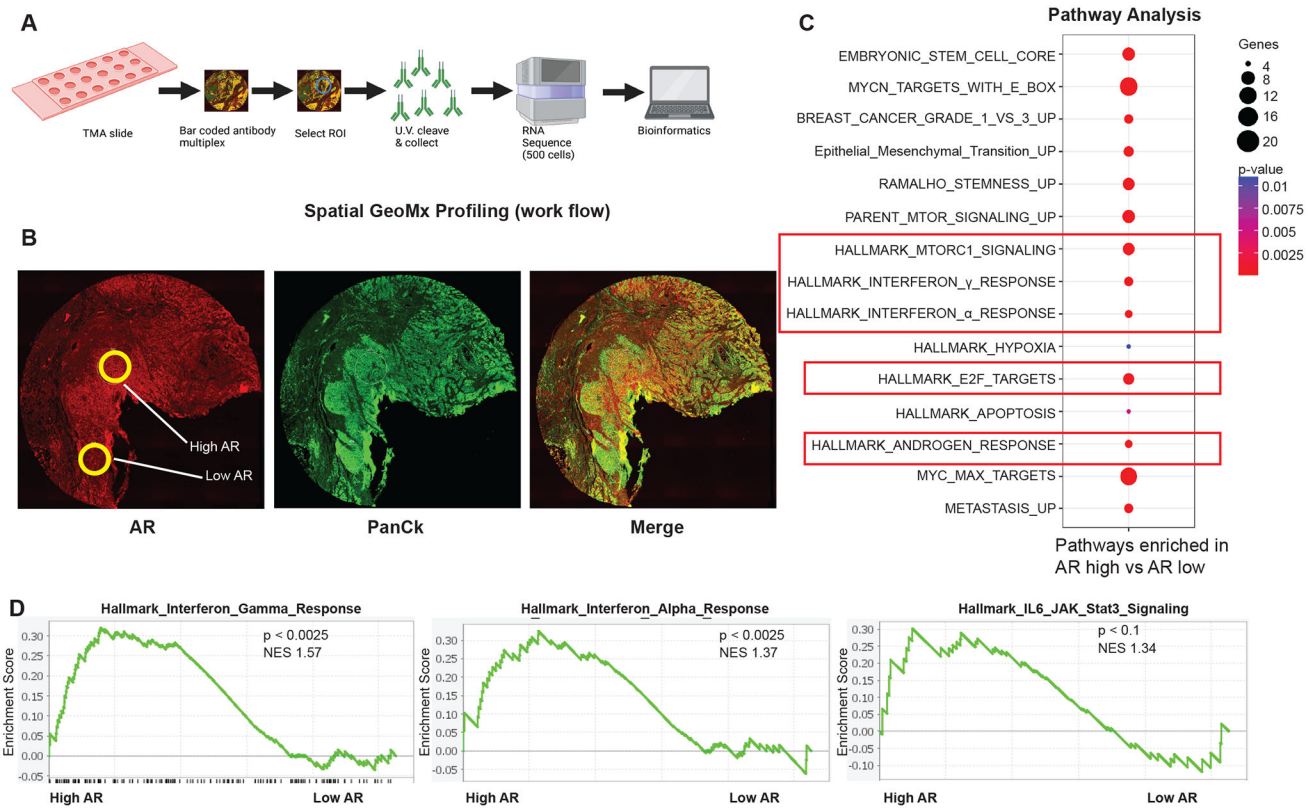

Figure 6. Spatial transcriptomics provides evidence that TNBC cells that express high AR have enriched interferon JAK-STAT pathway and aggressive phenotype cells compared to cells that express low AR.

A. A schematic of the Nanostring GeoMx spatial transcriptomics method (provided by Nanostring). **B**. Region of Interest (ROI) selection. LAR TNBC specimens (n=3) were stained for AR (red), PanCk (green), and DNA (blue). Regions that express AR at high levels compared to areas that express AR at low levels were selected as regions of interest. Cells were isolated using laser and sequenced. **C**. GSEA analysis shows enrichment of interferon JAK-STAT pathway. The top pathways enriched in AR high compared to AR low cells obtained from GSEA are shown as dot blot. **D**. Enrichment plots are shown for HALLMARK_INTERFERON_GAMMA_RESPONSE (left), HALLMARK_INTERFERON_ALPHA_RESPONSE (middle) and HALLMARK_IL6_JAK_STAT3_SIGNALING (right) pathways.

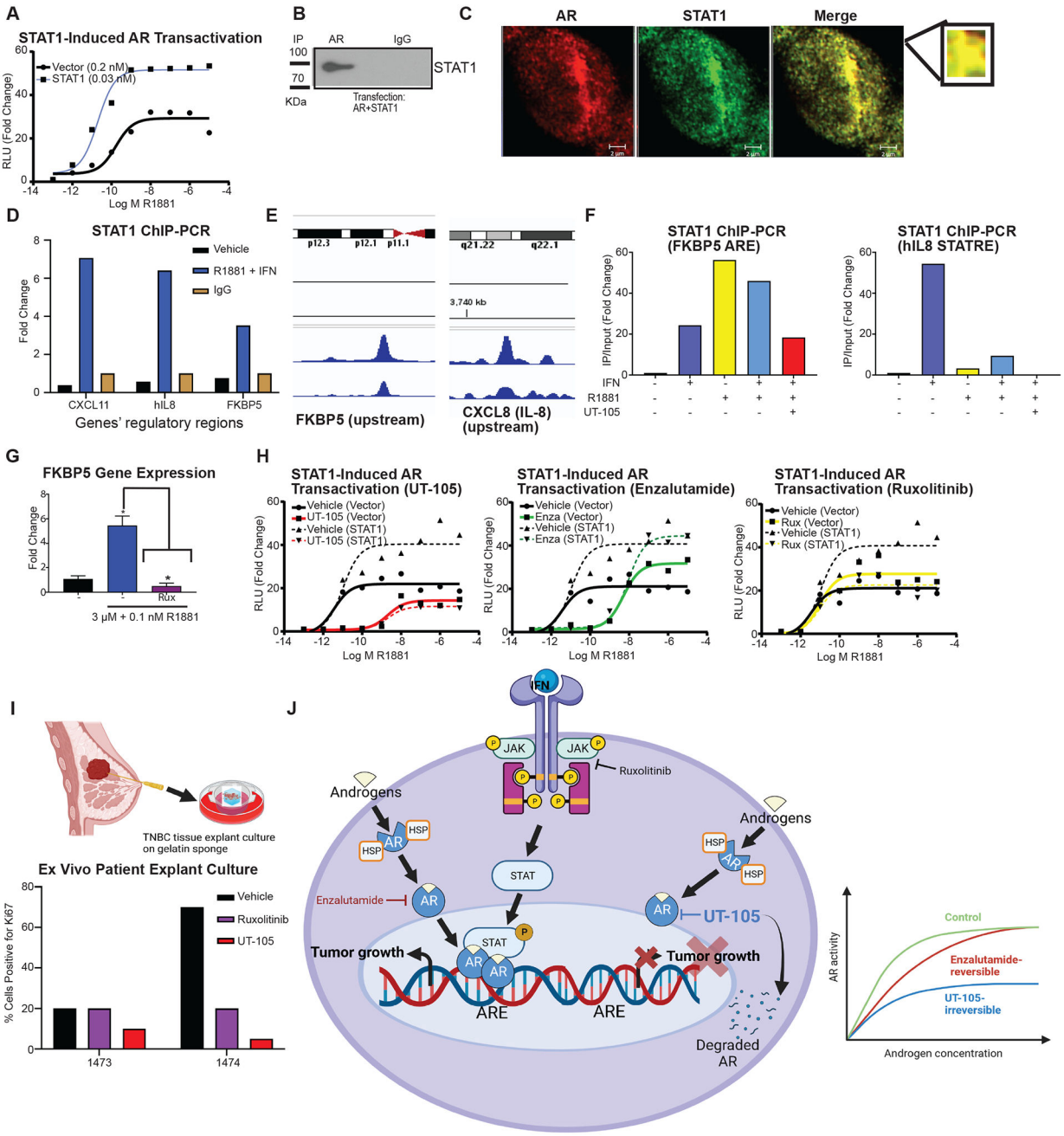

Figure 7. STAT1 is an AR coactivator.

A. STAT1 increases R1881-induced AR transactivation. AR transactivation was performed in HEK-293 cells with 0.1 μg vector or STAT1. Numbers provided in bracket are R1881's EC_{50} values. **B**. STAT1 and AR interact. AR and STAT1 (5 μg) were transfected into HEK-293 cells. Cells were treated 48 hours after transfection with 2000 IU interferon α and 10 nM R1881. Cells were harvested 4 hours after treatment, immunoprecipitation was performed with IgG or AR antibody, and Western blot was performed for STAT1. **C**. AR and STAT1 interact in MDA-MB-453 cells. MDA-MB-453 cells were maintained in charcoal-stripped serum-containing medium for two days and treated with interferon α and

R1881 for 4 hours. Cells were fixed and immunostained for AR (red) and STAT1 (green), and confocal microscopy was performed. Scale is 2 μm. **D**. STAT1 is recruited to ARE (on *FKBP5* regulatory region). MDA-MB-453 cells were treated as indicated. The cells were crosslinked, sheared, and ChIP PCR was performed with the STAT1 and IgG antibodies. PCR was performed using the primers for the indicated regions. **E**. AR is recruited to STAT1 responsive gene regulatory region. Data from AR ChIP-seq performed in PCa cells (n=2) were loaded in IGV browser and *CXCL8* (*IL8*) and *FKBP5* regulatory regions were scanned to determine the binding of AR. **F**. UT-105 inhibits STAT1 recruitment to STAT1RE and ARE. MDA-MB-453 cells maintained in charcoal-stripped serum-containing medium were treated with interferon α (1000 units), R1881 (1 nM), combination in the presence and absence of UT-105 (10 μM) for 4 hours. ChIP assay was performed with STAT1 antibody and real-time PCR was performed with primers specific for *hIL8* STATRE and *FKBP5* ARE. Representative experiment is shown in the figure. **G**. Ruxolitinib inhibits AR-target gene expression. MDA-MB-453 cells maintained in charcoal stripped serum-containing medium were treated with R1881 (0.1 nM) alone or in combination with ruxolitinib (3 μM) for 24 hours. RNA was extracted, and real-time PCR for *FKBP5* was performed (n=4/group; one-way ANOVA). **H**. UT-105 inhibits STAT1-dependent coactivation of AR. AR transactivation was performed in HEK-293 cells in the presence or absence of 0.1 μg STAT1. **I**. Effect of AR and JAK inhibitors on the proliferation of patient tumors explants growth. Illustration of gelatin sponge culture (Biorender.com). Tumor tissue from two patients (1473 and 1474) were placed on pre-soaked gelatin sponges and treated as indicated for 48 hours. The tissues were fixed and stained with Ki67. The bar graphs show the percentage of cells that stained positively for Ki67. **J**. ***Model***. A schematic of the proposed mechanism of action of SARDs in TNBC tumors (biorender.com). The model summarizes the choice of drug for inhibiting the growth of LAR TNBC tumors. This would depend on the specific mechanisms involved in AR activation and tumor progression. Enzalutamide may work if AR activity is the primary driver, but its efficacy could be limited by androgen surges. STAT inhibitors like ruxolitinib may not be effective if AR activation is independent of STAT1. Degraders like UT-105 seem promising as they degrade AR directly and could prevent AR or AR splice variant activation, offering a more comprehensive approach to inhibit tumor growth. However, the actual effectiveness of these drugs would need to be studied in clinical settings and may vary from patient to patient. Panels A-H representative of three independent experiments is shown.

Key resources table

REAGENT or RESOURCE	SOURCE	IDENTIFIER
Antibodies		
Anti-AR antibody (D6F11) XP	Cell Signaling	5153
Anti-AR-V7 antibody	Precision Antibody	AG10008 SQ3921368
Anti-AR-V7 antibody	Abcam	ab198394
Anti-GAPDH	Sigma	G8795
Rabbit and Mouse Secondary	ThermoFisher	PI31460
Anti-phospho-STAT1	Cell Signaling	9914T
Anti-phospho-STAT2	Cell Signaling	9914T
Anti-phospho-STAT3	Cell Signaling	9914T
Anti-phospho-JAK Family	Cell Signaling	32901S
Anti-phospho-AKT	Abcam	ab81283
STAT1 antibody	Cell Signaling	9172S
PanCytokeratin antibody	Novus clone AE1/AE3	NBP2–29429
Anti-AR antibody for IHC	Cell Signaling D6F11	5153
Anti-Estrogen receptor antibody for IHC	Leica biosystems	Clone 6F11
Bacterial and virus strains		
AR-V7 viral vector	Kind gift from Dr. Kris C. Wood and Dr. David M. Sabatini.	Martz CA et al., Sci. Signal 2014[53].
Biological samples		
52 TNBC Patient specimens	IRB 14–03113-XP UTHSC	N/A
PDX UT-1355	IRB 14–03113-XP UTHSC	N/A
Chemicals, peptides, and recombinant proteins		
Enzalutamide	Medkoo	201821
Bicalutamide	AK Scientific	90357–06-5
Ruxlotinib	AmBeed	A272323
Interferon	Gift from Dr. Pfeffer (which was a generous gift from Amgen)[84]	N/A
BrDU	Cell signaling	6813s
R1881	Sigma	R0908–10MG
Sypro Orange	Thermofisher	S6650
Matrigel	fisherscientific	8774552
Gelatin dental sponge (Vetspon Dental Cubes)	fisherscientific	NC0654350
Critical commercial assays		
Kinome Scan	DiscoverX Eurofins	N/A
GPCR Scan	DiscoverX Eurofins	N/A
Deposited data		
RNA Seq for MDA-MB-453 and MDA-MB-453-AR-V7	GEO database	GSE244283
Spatial genomics	GEO database	GSE245202

REAGENT or RESOURCE	SOURCE	IDENTIFIER
MDA-MB-453 xenograft	GEO database	GSE244283
41 patient specimens	GEO database	GSE244283
MDA-MB-453 cell line RNA sequencing	GEO database	GSE245554
Experimental models: Cell lines		
LNCaP	ATCC	CRL-1740
22RV1	ATCC	CRL-2505
MDA-MB-453	ATCC	HTB-131
MDA-MB-231	ATCC	CRM-HTB-26
BT549	ATCC	HTB-122
PC3	ATCC	CRL-1435
MFM223	Sigma Aldrich	SKU 98050130–1VL
Experimental models: Organisms/strains		
NSG mice	JAX labs	005557
Sprague Dawley rats	Charles River	N/A
Oligonucleotides		
TaqMan primers and probe Androgen Receptor N-terminus	Life Technologies	Hs00907242_m1
TaqMan primers and probe Androgen Receptor C-terminus	Life Technologies	Hs00171172_m1
TaqMan primers and probe *FKBP5*	Life Technologies	Hs00188025_m1
TaqMan primers and probe *TMPRSS2*	Life Technologies	Hs00237175_m1
TaqMan primers and probe *STEAP4*	Life Technologies	Hs01026584_m1
TaqMan primers and probe *IRF-1*	Life Technologies	Hs00971965_m1
TaqMan primers and probe *IRF-7*	Life Technologies	Hs01014809_g1
TaqMan primers and probe *IRF-9*	Life Technologies	Hs00196051_m1
TaqMan primers and probe *GAPDH*	Life Technologies	Hs00266705_g1
Primers and probe *AR-V7*	Custom synthesized	
Recombinant DNA		
STAT-1 plasmid	Gift from Dr. Pfeffer	N/A
Androgen receptor	Gift from Dr. Nancy Weigel, Baylor College of Medicine	N/A
GRE-LUC	Gift from Dr. Nancy Weigel, Baylor College of Medicine	N/A
Glucocorticoid receptor	Gift from Dr. Nancy Weigel, Baylor College of Medicine	N/A
Mineralocorticoid receptor	Gift from Dr. Nancy Weigel, Baylor College of Medicine	N/A
STAT-1RE LUC	James E. Darnell, Rockefeller University	N/A
AR-LBD bacterial expression vector	Constructed in our lab.	N/A
AF-1 bacterial expression vector	Constructed in our lab.	N/A
AR-V7 bacterial expression vector	Constructed in our lab.	N/A
Software and algorithms		

REAGENT or RESOURCE	SOURCE	IDENTIFIER
Other		